playing an important role in antiviral immunity. pDCs also produces IFN-α in response to nucleic acids derived from damaged self-tissues, and are thereby implicated in provoking inflammatory disorders such as lupus and psoriasis [2, 3]. Thus, pharmaceutical agents that suppress IFN-α production by pDCs are instrumental in elucidating mechanisms of the production of a large amount of IFN-α and in developing novel therapies for inflammatory disorders that involve pDCs.

A variety of protein kinases is involved in signaling pathways in immune responses. Antitumor kinase inhibitors that have different targets may be useful to dissect such pathways. Three tyrosine kinase inhibitors (TKIs), imatinib, nilotinib, and dasatinib, have been approved for the treatment of chronic myeloid leukemia (CML) and Philadelphia $(Ph)^+$ acute lymphoblastic leukemia (ALL), which are caused by constitutive activation of an ABL tyrosine kinase [4]. Notably, dasatinib is capable of inhibiting a broad array of tyrosine kinases in addition to ABL, among which SRC family kinases (SFKs) are prominent targets [5]. As a consequence, it has been shown that dasatinib inhibits activation of T cells [6, 7] and NK cells [8, 9] in vitro. However, it has not been reported whether dasatinib affects immunostimulatory activity of DCs, which play a pivotal role in the induction of innate and adaptive immune responses.

Here, we investigated the effect of dasatinib on human pDCs in comparison with the effects of the other TKIs, imatinib, and nilotinib [10]. We show that clinically relevant concentrations of dasatinib, but not imatinib or nilotinib, strongly suppressed the production of IFN-α and proinflammatory cytokines by pDCs without impairing viability. Mechanistic analysis suggests that dasatinib suppresses IFN-α production by pDCs through inhibiting both SFK-dependent pathways and SFK-independent endosomal retention of CpG DNA, which is a critical step for pDCs to produce a large amount of IFN-α [11, 12]. These results have significant implications for dissecting the mechanisms of IFN-α production by pDCs and for developing novel therapies for pDC-related inflammatory disorders.

Results

Dasatinib suppresses cytokine production by pDCs stimulated with TLR9 and TLR7 ligands

There are two major types of CpG oligodeoxynucleotides (ODNs), CpG-A, and CpG-B [13]. CpG-A forms large multimeric aggregates, whereas CpG-B are monomeric and do not form such high order structure [14]. CpG-A shares its particle-like physical features with viral particles and an aggregated self-DNA-antimicrobial peptide complex observed in psoriatic lesions [15]. These particle-like nucleic acids induce pDCs to produce a large amount of IFN-α due to their prolonged retention in early endosomes [11, 12]. Thus, we first examined whether dasatinib suppresses IFN-α production by pDCs stimulated with two TLR9 ligands, ODN2216 (CpG-A) or HSV-1. We also stimulated pDCs with a TLR7 ligand, influenza virus, which similarly induces a large amount of IFN-α production by pDCs. When we stimulated PBMCs depleted of pDCs with ODN2216, IFN-α was scarcely detected in the supernatant (Supporting Information Fig. 1), indicating that pDCs are virtually the only cell type among PBMCs that secretes a detectable level of IFN-α in response to CpG-A. Thus, we pretreated PBMCs for 1 h with one of the three ABL kinase inhibitors dasatinib, imatinib, and nilotinib at clinically relevant concentrations observed in blood after administration. We then added the TLR ligands to each condition and cultured PBMCs for 24 h, and concentrations of IFN-α in the supernatants were measured by ELISA (Fig. 1A). Dasatinib strongly suppressed IFN-α production by pDCs stimulated with ODN2216 as well as natural ligands, HSV-1 or influenza virus, in a dose-dependent manner, and a low concentration (10 nM) was sufficient to induce significant suppression. Imatinib and nilotinib suppressed the IFN-α production to a lesser extent, and high concentrations (5000 and 1000 nM) were necessary to exhibit substantial suppression. When we calculated absolute amounts of IFN-α secreted from a single pDC, we obtained similar results (Supporting Information Fig. 2).

We also examined the effect of dasatinib on IFN-α production by purified pDCs to exclude indirect effects from other cell types. Dasatinib suppressed the production of IFN-α by purified pDCs, whereas imatinib did so to a lesser extent (Fig. 1B), as observed with PBMCs.

Whereas CpG-A induces pDCs to produce both IFN-α and proinflammatory cytokines (TNF-α and IL-6), CpG-B induces production of TNF-α and IL-6 but only a low level of IFN-α [16]. Thus, we next examined whether dasatinib suppresses cytokine production by pDCs stimulated with ODN2216 (CpG-A) or ODN2006 (CpG-B) to compare the suppressive effect of dasatinib on the two types of CpG DNA. Dasatinib strongly suppressed production of IFN-α, TNF-α, and IL-6 induced by ODN2216 (Fig. 1C). In contrast, dasatinib significantly suppressed IFN-α and TNF-α production induced by ODN2006 only at a high concentration (100 nM), and did not suppress IL-6 production (Fig. 1C). Dasatinib reduced the frequency of pDCs bearing intracellular IFN-α and TNF-α (Supporting Information Fig. 3), excluding the possibility that dasatinib simply blocks secretion of the cytokines. In addition, dasatinib suppressed upregulation of CD86 induced by ODN2216 but not by ODN2006 (Supporting Information Fig. 4). Dasatinib also suppressed IL-6 production induced by HSV-1 and influenza virus (Supporting Information Fig. 5).

Neither dasatinib nor imatinib significantly reduced the viability of pDCs stimulated with ODN2216 or ODN2006 (Supporting Information Fig. 6).

Collectively, these data indicate that dasatinib strongly suppresses the production of IFN-α, TNF-α, and IL-6 and the expression of CD86 by pDCs stimulated with CpG-A or natural viral ligands but not with CpG-B without reducing viability.

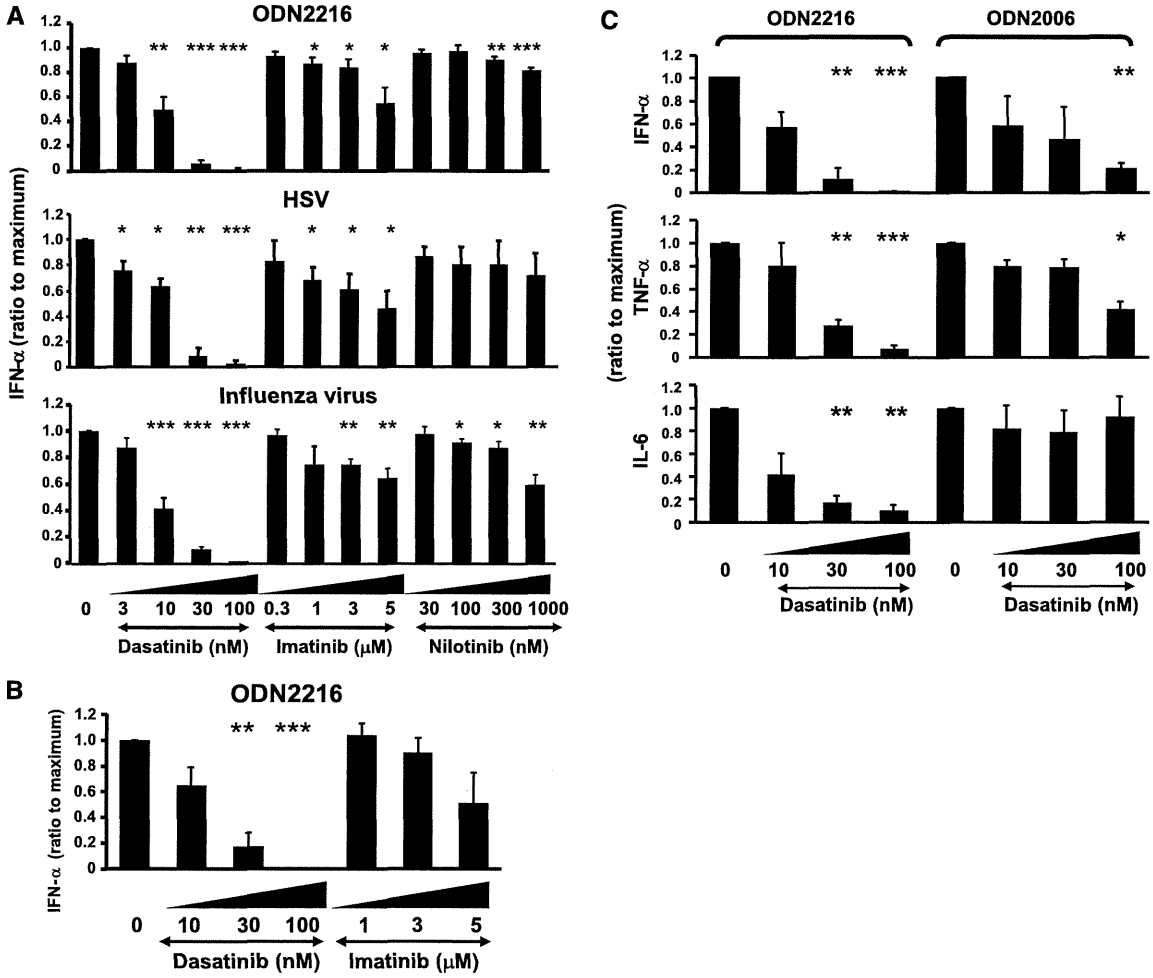

Figure 1. Dasatinib suppresses production of IFN-α and proinflammatory cytokines by pDCs stimulated with CpG-A or viruses. (A) PBMCs were stimulated with ODN2216, HSV-1, or influenza virus in the absence or presence of the indicated concentrations of TKIs for 24 h. The concentration of IFN-α in the supernatants was measured in duplicate by ELISA. Because the absolute concentrations were variable depending on the donors, the cytokine concentrations were normalized to the maximum value obtained without the TKIs. The data are shown as means + SE of 7 (ODN2216), 3 (HSV-1), or 6 (influenza virus) independent experiments. $^{*}p < 0.05$, $^{**}p < 0.01$, $^{***}p < 0.001$ between the data obtained without TKIs and those obtained with each concentration of TKIs, paired two-tailed *t*-test. The means and ranges of absolute concentrations of IFN-α obtained without TKIs are as follows: ODN2216 3874 pg/mL (703–9619 pg/mL); HSV-1 3014 pg/mL (632–5262 pg/mL); influenza virus 5334 pg/mL (2117–10 764 pg/mL). (B) Purified pDCs were stimulated with ODN2216 in the absence or presence of the indicated concentrations of TKIs for 24 h. The concentration of IFN-α in the supernatants was measured in duplicate by ELISA, and normalized to the maximum value obtained without TKIs. The data are shown as means + SE of four experiments. $^{**}p < 0.01$, $^{***}p < 0.001$, paired two-tailed *t*-test. The mean and range of absolute concentrations of IFN-α obtained without TKIs are 62 960 pg/mL (34 078–85 289 pg/mL).(C) Purified pDCs were stimulated with ODN2216 (CpG-A) or ODN2006 (CpG-B) in the absence or presence of the indicated concentrations of dasatinib for 24 h. The concentrations of IFN-α, TNF-α, and IL-6 in the supernatants were measured in duplicate by ELISA, and normalized to the maximum value obtained without dasatinib. The data are shown as means + SE of 4 (IFN-α) and 3 (TNF-α, IL-6) independent experiments. $^{*}p < 0.05$, $^{**}p < 0.01$, $^{***}p < 0.001$, paired two-tailed *t*-test. The means and ranges of absolute concentrations of IFN-α obtained without dasatinib are as follows: ODN2216 62 960 pg/mL (34 078–85 289 pg/mL); ODN2006 398 pg/mL (66–822 pg/mL). TNF-α: ODN2216 1443 pg/mL (1026–1935 pg/mL); ODN2006 849 pg/mL (750–915 pg/mL). IL-6: ODN2216 3883 pg/mL (2173–5160 pg/mL); ODN2006 4156 pg/mL (1483–7571 pg/mL).

Dasatinib reduces the IFN-α-producing capacity of pDCs in vivo

To examine whether administration of dasatinib also reduce the IFN-α-producing capacity of pDCs in vivo, we stimulated PBMCs from patients of CML or Ph^+ ALL with ODN2216 before starting dasatinib (100 mg once a day) or nilotinib (400 mg twice a day) and two time points after starting them, and measured concentrations of IFN-α in the supernatants by ELISA. Because the proportion of pDCs among PBMCs may vary during the clinical course in each patient, we calculated absolute amounts of IFN-α secreted from a single pDC to exclude the influence of fluctuations of the pDC frequency. Information of the patients is described in Supporting Information Table 1. Dasatinib but not nilotinib significantly reduced the IFN-α-producing capacity of pDCs (Fig. 2). This indicates that

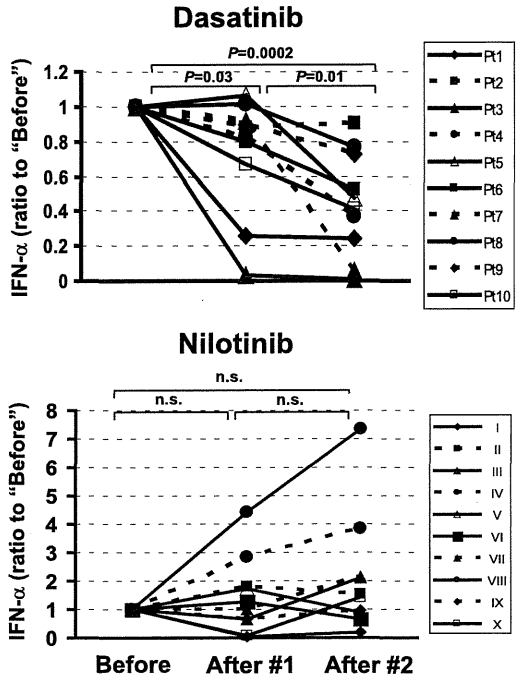

Figure 2. Dasatinib suppresses IFN-α production by pDCs in patients with CML and Ph+ ALL. PBMCs were obtained from 17 CML patients and 3 Ph+ ALL patients (ten patients for dasatinib and nilotinib each) at three time points (before starting dasatinib or nilotinib ("before"), 2–3 weeks after starting the drugs ("after #1"), 4–8 weeks after starting the drugs ("after #2")). PBMCs were stimulated with ODN2216 for 24 h. The concentration of IFN-α in the supernatants was measured by ELISA, and the absolute amounts of IFN-α secreted from a single pDC were calculated. The amounts of IFN-α after starting dasatinib or nilotinib were normalized to the control value obtained before starting them. Statistical significance was determined by paired two-tailed t-test. n.s.: not significant. The means and ranges of the amounts of IFN-α before starting dasatinib or nilotinib are as follows: dasatinib 0.39 pg (0.02–0.92 pg); nilotinib 0.25 pg (0.04–0.63 pg).

dasatinib suppresses the IFN-α-producing capacity of pDCs in vivo as well.

SFK inhibitors suppress IFN-α production by pDCs stimulated with CpG-A

Next, we investigated mechanisms by which dasatinib suppresses cytokine production by pDCs. Because dasatinib strongly suppresses SFKs [5], we examined whether SFK inhibitors PP2 [17] and SU6656 [18], suppress the production of IFN-α, TNF-α, and IL-6 by pDCs stimulated with ODN2216. Whereas PP2 and SU6656 did not significantly reduce the viability of pDCs (data not shown), these reagents suppressed the cytokine production in a dose-dependent manner (Fig. 3A). In contrast, PP2 did not suppress TNF-α and IL-6 production induced by ODN2006, and SU6656 significantly did so only at the highest concentration (Fig. 3B). Thus, it is likely that inhibition of SFKs is responsible for the suppressive effect of dasatinib on pDCs stimulated with CpG-A at least in part.

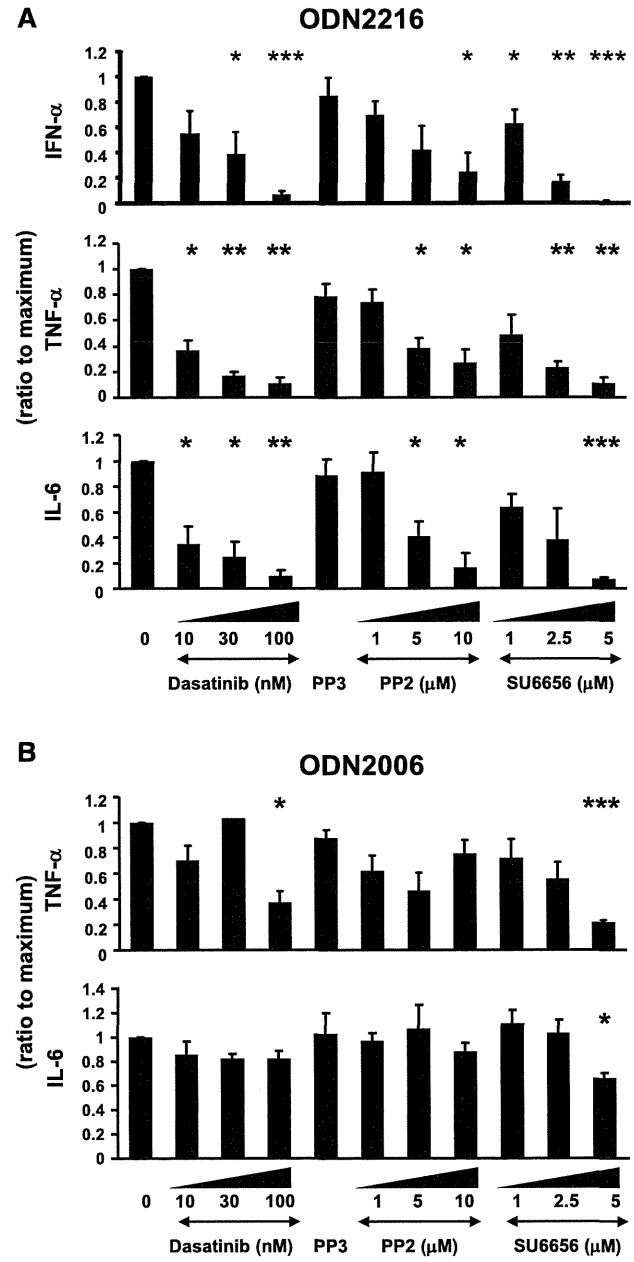

Figure 3. SFK inhibitors suppress production of IFN-α and proinflammatory cytokines by pDCs stimulated with CpG-A. (A) Purified pDCs were stimulated with ODN2216 in the absence or presence of the indicated concentrations of inhibitors or 10 μM PP3 for 24 h. The concentrations of IFN-α, TNF-α, and IL-6 in the supernatants were measured in duplicate by ELISA, and normalized to the maximum value obtained without the inhibitors. The data are shown as means + SE of four (IFN-α) and three (TNF-α, IL-6) experiments. $^{*}p < 0.05$, $^{**}p < 0.01$, $^{***}p < 0.001$ between data obtained without kinase inhibitors and those obtained with each concentration of inhibitors, paired two-tailed t-test. The mean and range of absolute concentrations of IFN-α, TNF-α, and IL-6 obtained without the inhibitors are 55 157 pg/mL (26 553–12 1608 pg/mL), 421 pg/mL (194–590 pg/mL), and 2059 pg/mL (783–4389 pg/mL), respectively. (B) Purified pDCs were stimulated with ODN2006 in the absence or presence of the inhibitors for 24 h. The concentrations of TNF-α and IL-6 in the supernatants from three experiments were analyzed as in (A). The mean and range of absolute concentrations of TNF-α and IL-6 obtained without the inhibitors are 263 pg/mL (70–598 pg/mL) and 1027 pg/mL (427–1902 pg/mL), respectively.

Dasatinib inhibits nuclear translocation of IRF7 and NF-κB in pDCs stimulated with CpG-A

The earliest event leading to CpG ODN-induced IFN-α production is endocytosis of CpG ODN by pDCs. Thus, we examined whether dasatinib inhibits uptake of CpG ODN by pDCs. We observed the intracellular localization of FITC-conjugated ODN2216 in the absence or presence of dasatinib by confocal microscopy (Supporting Information Fig. 7). Whereas pDCs kept on ice did not endocytose ODN2216, pDC cultured at 37°C did. Dasatinib did not inhibit the endocytosis of ODN2216. Thus, dasatinib targets a signaling pathway(s) further downstream.

Upon stimulation with CpG ODN, TLR9 rapidly moves from the ER to endosomes [19]. We have recently shown that a proteasome inhibitor bortezomib inhibits the intracellular trafficking of TLR9 in pDCs [20]. Thus, we next examined whether dasatinib also inhibits this step. We stimulated purified pDCs with ODN2216 in the absence or presence of dasatinib, and examined whether TLR9 colocalizes with an ER marker (ER-Tracker) or early endosomal markers (EEA1 and Rab5) by confocal microscopy. To quantitatively compare the degrees of colocalization between culture conditions, we analyzed the data using Manders' Colocalization Coefficients [21,22] with the Costes' method of automatic thresholding [22,23]. Supporting Information Fig. 8A and B shows representative confocal images and statistical analysis of pooled microscopy data, respectively. TLR9 colocalized with ER-Tracker but not with EEA1 or Rab5 without stimulation. In contrast, TLR9 did not colocalize with ER-Tracker and instead colocalized with EEA1 and Rab5 after stimulation with ODN2216, indicating trafficking of TLR9 from the ER to early endosomes. TLR9 also colocalized with EEA1 and Rab5 but not with ER-Tracker even in the presence of dasatinib. Thus, dasatinib does not inhibit the trafficking of TLR9 from the ER to endosomes induced by CpG ODN.

Stimulation of pDCs with CpG ODN induces the nuclear translocation of two major transcription factors, IFN regulatory factor (IRF)7 and NF-κB [24]. IRF7 and NF-κB induce the production of IFN-α and proinflammatory cytokines at the final step of TLR signaling, respectively. Thus, we examined whether dasatinib inhibits the nuclear translocation of these transcription factors induced by ODN2216 in pDCs. Whereas IRF7 and NF-κB are located in the cytoplasm in untreated pDCs, both of the transcription factors moved to the nucleus after stimulation with ODN2216 (Fig. 4). Dasatinib inhibited the nuclear translocation of IRF7 and NF-κB, consistently with the suppression of production of IFN-α and proinflammatory cytokines induced by ODN2216.

Dasatinib and a SFK inhibitor inhibit intracellular events upstream of TLR9 engagement

Intracellular events after endocytosis of CpG DNA resulting in the nuclear translocation of transcription factors are composed of (i) trafficking of endosomes carrying CpG DNA (upstream of TLR9) and (ii) signaling triggered by TLR9 engagement (downstream of TLR9). Chloroquine suppresses CpG-induced cellular activation by inhibiting endosomal acidification and thus cleavage of the ectodomain of TLR9 necessary for downstream signaling [25], resulting in suppression of IFN-α production by pDCs (data not shown). Thus, we compared the effects of the three TKIs, PP2, and chloroquine on CpG-induced IFN-α production and tyrosine phosphorylation in pDCs. Because we could not extract sufficient amounts of proteins from primary pDCs to obtain unambiguous results in Western blotting, we used a cell line derived from blastic pDC neoplasm, CAL-1 [26]. As mixing ODN2216 with cationic liposome 1,2-dioleoyloxy-3-trimethylammonium-propane (DOTAP) was necessary to induce CAL-1 to produce IFN-α, we stimulated CAL-1 with the mixture of ODN2216 and DOTAP. Dasatinib, PP2, and chloroquine suppressed IFN-α production by CAL-1, as they did for primary pDCs (Supporting Information Fig. 9A). The stimulation induced tyrosine phosphorylation of several proteins (Supporting Information Fig. 9B). Chloroquine did not inhibit the phosphorylation, indicating that the tyrosine phosphorylation induced by CpG DNA occurs upstream of TLR9 engagement. In contrast, dasatinib, but not imatinib or nilotinib, inhibited the phosphorylation in a dose-dependent manner. PP2 also did so. These data suggest that dasatinib and PP2 inhibit intracellular events upstream of TLR9.

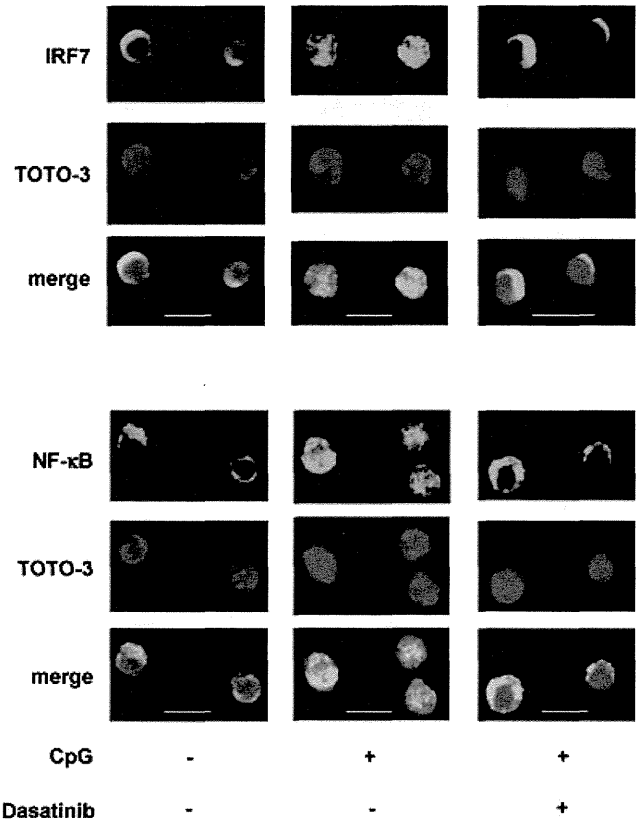

Figure 4. Dasatinib inhibits the nuclear translocation of IRF7 and NF-κB in pDCs.Purified pDCs were stimulated with ODN2216 in the absence or presence of dasatinib for 24 h. The cells were stained with rabbit anti-IRF7 (top) or anti-NF-κBp65 (bottom, both green). Nuclei were identified using TOTO-3 dye (blue). The data shown are representative of three experiments performed. Scale bars, 10 μm.

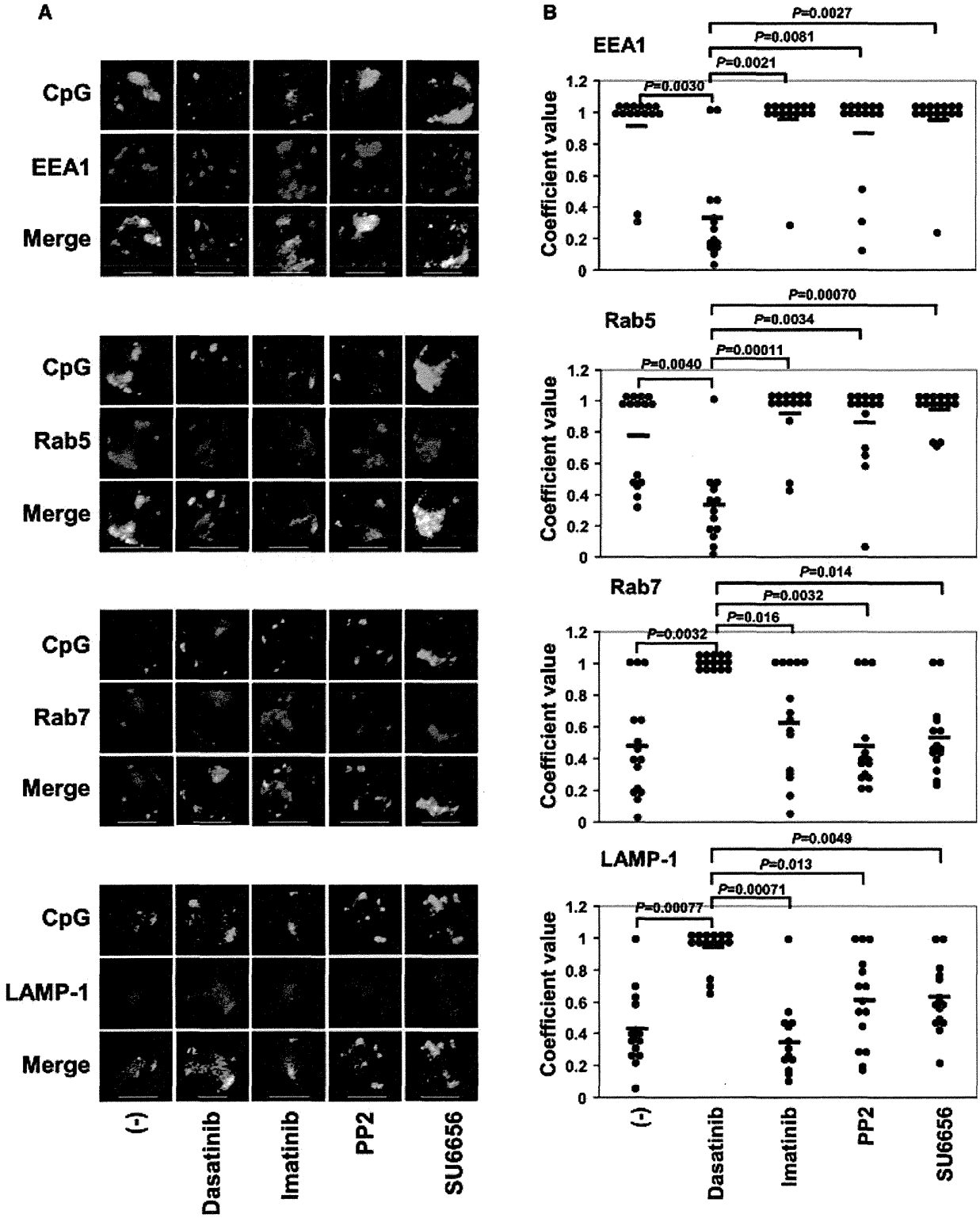

Figure 5. Dasatinib, but not SFK inhibitors, inhibits the retention of CpG-A in early endosomes. Purified pDCs were cultured with FITC-conjugated ODN2216 in the absence or presence of the TKIs or the SFK inhibitors for 90 min. The cells were stained with anti-EEA1 or anti-Rab5 mAb for early endosomes, or anti-Rab7 mAb for late endosomes, followed by Alexa Fluor 555-conjugated goat anti-rabbit IgG. Alternatively, the cells were stained with PE-conjugated mouse anti-LAMP-1 mAb for late endosomes and lysosomes. (A) Data shown are representative of three to five experiments. Positive signals for both probes are shown in white. Scale bars, 5 μm. (B) Statistical analysis of microscopy data pooled from three to –five experiments. Each symbol represents a cell, and 15 cells were analyzed for each condition. The coefficient value represents the fraction of green in compartments containing red. Statistical significance was determined by Mann–Whitney *U*-test with Bonferroni correction following Kruskal–Wallis *H*-test.

Dasatinib, but not SFK inhibitors, abrogates retention of CpG-A in early endosomes

It has been shown that CpG-A is retained in early endosomes together with the MyD88-IRF7 complex for a long period in pDCs but not in conventional DCs [11, 12]. This spatiotemporal regulation of CpG trafficking is likely to enable prolonged activation of the signaling complex, leading to prodigious production of IFN-α by pDCs. Thus, we examined whether the TKIs (dasatinib, imatinib) and the SFK inhibitors (PP2, SU6656) affect trafficking of endosomes carrying CpG-A in pDCs by confocal microscopy. We used EEA1 and Rab5 as early endosome markers, Rab7 as a late endosome marker, and LAMP-1 as a lysosome marker. Figure 5A and B shows representative confocal images and statistical analysis of pooled microscopy data, respectively. ODN2216 colocalized with EEA1 and Rab5 rather than with Rab7 and LAMP-1 without any of the inhibitors, indicating retention of ODN2216 in early endosomes. Notably, ODN2216 colocalized with Rab7 and LAMP-1 rather than with EEA1 and Rab5 in the presence of dasatinib, indicating that dasatinib abrogates the retention of ODN2216 in early endosomes. In contrast, ODN2216 remained colocalized with EEA1 and Rab5 in the presence of imatinib. Unexpectedly, ODN2216 also remained colocalized with EEA1 and Rab5 in the presence of PP2 or SU6656, indicating that the SFK inhibitors as well as imatinib do not abrogate the retention of ODN2216 in early endosomes. Collectively, these data suggest that dasatinib, but not imatinib, abrogates retention of CpG-A in early endosomes and facilitates trafficking to late endosomes and lysosomes in pDCs by inhibiting protein kinases other than SFKs.

Discussion

pDCs represent a unique immune cell type in that they rapidly produce a vast amount of IFN-α in response to nucleic acids derived not only from pathogens but also from damaged self-cells. Here, we showed that a TKI dasatinib potently suppresses IFN-α production by pDCs without reducing cell viability. Importantly, dasatinib abrogated retention of CpG-A in early endosomes and facilitated the movement of CpG-A to late endosomes/lysosomes. It is of note that this effect is independent of SFKs. This is the first study showing the pharmacological interruption of the critical step for pDCs to produce IFN-α: prolonged localization of CpG DNA in early endosomes [11, 12]. It sheds new light on the molecular mechanisms by which pDCs perform their immune functions and on the development of novel therapies for pDC-related inflammatory disorders.

Among the three TKIs (dasatinib, imatinib, nilotinib), dasatinib most strongly suppressed IFN-α production by pDCs stimulated with representative IFN-α inducers, ODN2216 (CpG-A), HSV-1 (TLR9 ligand), or influenza virus (TLR7 ligand) at clinically relevant, low concentrations. Although imatinib and nilotinib also diminished IFN-α production, the effects were much weaker than that of dasatinib and needed high concentrations. Dasatinib also potently suppressed production of TNF-α and IL-6 as well as expression of CD86 by pDCs stimulated with ODN2216 (CpG-A). However, the suppression of such responses induced by ODN2006 (CpG-B) was less marked. The main difference between CpG-A and CpG-B is in the mode of their endosomal transport; CpG-A is retained in early endosomes for a longer time than CpG-B [11, 12]. Thus, the differential effects of dasatinib on the stimulation with CpG-A and CpG-B imply that dasatinib may target certain functions of early endosomes.

Importantly, dasatinib, but not nilotinib, significantly diminished the IFN-α-producing capacity of pDCs in patients treated with these drugs. These data are consistent with the in vitro data, and suggest that dasatinib suppresses the IFN-α-producing capacity of pDCs in vivo as well.

Next, we examined the mechanisms by which dasatinib suppresses cytokine production by pDCs stimulated with CpG-A. Two inhibitors of SFKs (PP2, SU6656) significantly suppressed production of IFN-α, TNF-α, and IL-6 by pDCs stimulated with CpG-A but not with CpG-B, consistent with the previous report [27]. Correspondingly, dasatinib and PP2 suppressed CpG-triggered global tyrosine phosphorylation in a pDC cell line CAL-1, but chloroquine did not, suggesting that dasatinib and PP2 inhibits CpG-induced intracellular events upstream of TLR9. Notably, however, dasatinib but not PP2 or SU6656 abrogated prolonged localization of CpG-A in early endosomes, and facilitated transport of CpG-A to late endosomes/lysosomes. These data suggest that dasatinib suppresses IFN-α production by pDCs through inhibiting both SFK-dependent and SFK-independent signaling pathways. Although both of the pathways appears to be involved in the functions of early endosomes necessary for responses to CpG-A, the data of confocal microscopy indicates that only the SFK-independent pathway is responsible for the prolonged localization of CpG-A in early endosomes.

The mechanisms by which an aggregated form of CpG DNA is retained in early endosomes in pDCs for a long period remain to be elucidated. It has been shown that an aggregated form of CpG DNA rapidly goes to late endosomes/lysosomes in conventional DCs in mice [11], suggesting that pDCs have distinctive mechanisms for retention of CpG DNA in early endosomes. A wide variety of protein kinases is involved in endocytic pathways [28]. Dasatinib targets a broad array of tyrosine kinases and several serine/threonine kinases [29–32]. Thus, dasatinib may affect endosomal trafficking in pDCs by inhibiting certain protein kinases other than SFKs involved in early-to-late endosome transition.

In this context, two recent studies have shown that the machinery of lysosome-related organelle biogenesis is essential for TLR7 and TLR9 signaling in pDCs but not in conventional DCs. Sasai et al [33] have reported that the adaptor protein (AP)-3 complex is responsible for trafficking of TLR9 to IRF7$^+$ endosomes but not to NF-κB$^+$ endosomes using mouse macrophages, and that AP-3 is necessary for the production of IFN-α but not IL-12 by mouse pDCs. Blasius et al. [34] have reported that an oligopeptide transporter Slc15a4 and three protein complexes involved in Hermansky–Pudlak syndrome (AP-3, biogenesis of lysosome-related organelles complex (BLOC)-1, BLOC-2) are required for production of both IFN-α and proinflammatory cytokines by pDCs

stimulated with TLR7 or TLR9 ligands. Slc15a4 [35] and the three complexes [36] are located in early endosomes, and BLOC-1 is necessary for sorting certain cargoes from early endosomes to lysosome-related organelles [37]. Together with these findings, the present study suggests that distinctive properties of early endosomes in pDCs, which is affected by dasatinib, are crucial for the large amount of IFN-α production. Although vesicle traffic pathways for TLR7 ligands to induce IFN-α has not been reported, the involvement of Slc15a4 [34] and AP-3 [33] in type I IFN production by pDCs stimulated with TLR7 ligands suggests that dasatinib targets similar machineries for IFN-α induction by TLR7 and TLR9 ligands.

In conclusion, dasatinib strongly suppresses the production of IFN-α and proinflammatory cytokines by pDCs stimulated with CpG-A, most likely by inhibiting both SFK-dependent and independent pathways, the latter of which is responsible for the prolonged localization of an aggregated form of CpG DNA in early endosomes. Protein phosphorylation is at the heart of controlling the physical properties of endocytosis and of integrating them with signal transduction networks of the cell [28]. Thus, the present study provides a clue to dissect molecular mechanisms for the distinctive behavior of endosomes in pDCs as well as possibilities to develop novel therapies for inflammatory disorders by targeting the endosomal trafficking in pDCs.

Materials and methods

Culture media and reagents

RPMI 1640 (Wako, Osaka, Japan) supplemented with 10% heat-inactivated FBS (Equitec-Bio, Inc., Kerrville, TX, USA), 2 mM L-glutamine, penicillin G, streptomycin (Gibco BRL, Carlsbad, CA, USA), and 10 mM HEPES (Nacalai Tesque, Kyoto, Japan) were used for cell culture. Dasatinib (provided by Bristol-Myers Squibb Company), imatinib, and nilotinib (provided by Novartis Pharma) were dissolved in DMSO (Nacalai Tesque) at 100 mM as a stock solution and were stored at −20°C. A SFK inhibitor PP2 and its negative control PP3 were purchased from Calbiochem (Darmstadt, Germany), and a SFK inhibitor SU6656 was purchased from Cayman Chemical (Ann Arbor, MI, USA). HSV-1 (KOS strain, a gift from Dr. Masaki Yasukawa (Ehime University, Ehime, Japan)) was attenuated with UV irradiation. Influenza virus ($10^{5.3}$ median tissue culture infective dose/0.2 mL of A/Niigata/05F254/2006, a kind gift from Dr. Reiko Saito (Niigata University, Niigata, Japan)) was inactivated at 56°C for 30 min. A cell line derived from blastic plasmacytoid dendritic cell neoplasm CAL-1 was described previously by Maeda et al. [26].

Isolation of pDCs

This study was approved by the Institutional Review Board of the Graduate School of Medicine at Kyoto University and abides by the tenets of the Declaration of Helsinki. PBMCs were obtained from healthy donors with written informed consent. $CD4^+CD11c^-lin^-$ cells were isolated as pDCs as described [38], using FACSAria cell sorter (BD Biosciences, San Jose, CA, USA). Reanalysis of the sorted cells confirmed a purity of more than 98%.

Cell culture

PBMCs were plated in flat-bottom, 96-well plates at 4×10^5 cells/200 μL. Purified pDCs were plated in round-bottom, 96-well plates at 4×10^4 cells/200 μL, except culture for stimulation with ODN2006 where the cells were plated at 1×10^5 cells/200 μL. The cells were pretreated with indicated concentrations of TKIs or SFK inhibitors for 1 h, and were stimulated with 0.5 μM ODN2216 (CpG-A) [16], ODN2006 (CpG-B) [39] (Operon Biotechnologies, Huntsville, AL, USA), 10^6 PFU/mL HSV-1, or 0.5% vol/vol influenza virus without removing the inhibitors for 24 h. For control culture, DMSO was added instead of the inhibitors. The cells were used for flow cytometry, and the supernatants were used for ELISA. For confocal analyses, pDCs were cultured for indicated time periods.

Analysis of cell viability

The cultured pDCs were stained with FITC-conjugated CELL LAB ApoScreen annexin V (Beckman Coulter, Orange County, CA, USA) and propidium iodide, and were analyzed for viability by flow cytometry with the FACSCalibur, and data were analyzed with CellQuest software (BD Biosciences).

Analysis of cytokine production by ELISA

Concentrations of cytokines in the supernatants were measured by ELISA. The following reagents were used: the human IFN-α module set (Bender MedSystems, Vienna, Austria) and the human TNF-α and IL-6 ELISA MAX Standard sets (BioLegend, San Diego, CA, USA).

Analysis of patient samples

Peripheral blood samples were obtained from 17 CML (chronic phase) patients and three Ph^+ ALL patients who newly started dasatinib or nilotinib, at three time points (before, 2–3 weeks after, and 4–8 weeks after starting dasatinib or nilotinib) under the approval by the Institutional Review Board of the Graduate School of Medicine at Kyoto University and with written informed consent. PBMCs isolated with Lympholyte-H (CEDARLANE, Burlington, Ontario, Canada) were stained with FITC-conjugated

anti-BDCA-2 (CD303) mAb (Miltenyi Biotec, Bergisch Gladbach, Germany), and pDCs were identified as BDCA-2$^+$ cells with the FACSCalibur. Dead cells were excluded by staining with propidium iodide. Absolute numbers of pDCs in the wells were calculated from numbers of PBMCs and percentages of BDCA-2$^+$ cells among PBMCs. The PBMCs were cultured in flat-bottom, 96-well culture plates at 4×10^5 cells/200 μL in the presence of 0.5 μM ODN2216 for 24 h. Culture supernatants were analyzed for concentrations of IFN-α by ELISA. The amounts of IFN-α secreted from a single pDC were calculated by dividing the amounts of IFN-α in the supernatants by absolute numbers of pDCs.

Western blotting

CAL-1 cells were pretreated for 1 h with 10 μM PP3, 10 μM PP2, 10 μM chloroquine (WAKO), 5 μM imatinib, 1 μM nilotinib, or indicated concentrations of dasatinib. The cells were stimulated with DOTAP Liposomal Transfection Reagent (Roche Applied Science, Penzberg, Germany) alone or 1 μM ODN2216 plus DOTAP for 1 h without removing the inhibitors. The cells were lysed directly in sample buffer containing 1%SDS, boiled, and diluted tenfold with 1% Triton X-100-containing lysis buffer. The cell extracts were fractionated by SDS-PAGE and transferred to Immobilon-P transfer membranes (Millipore, Billerica, MA, USA), using a wet transfer apparatus (Bio-Rad Laboratories, Hercules, CA, USA). The membranes were incubated with HRP-conjugated anti-phosphotyrosine mAb (PY20) (Transduction Laboratories, Lexington, KY, USA) or anti-β-actin mAb (Sigma, St. Louis, MO, USA) for 1 h. After a wash with TBS-T (25 mM Tris-HCl (pH 7.4), 137 mM NaCl, 2.7 mM KCl, and 0.1% Tween 20), peroxidase activity was detected with Pierce Western Blotting Substrate (Thermo Scientific, Waltham, MA, USA).

Confocal microscopy

To observe uptake of CpG ODN, purified pDCs were cultured in the absence or presence of 100 nM dasatinib for 1 h, and were incubated with 6 μM FITC-conjugated ODN2216 (InvivoGen, San Diego, CA, USA) for 3 h without removing dasatinib. The cells were harvested, washed, stained with PE-conjugated anti-HLA-DR mAb (BD Biosciences), and fixed with 2% paraformaldehyde. pDCs cultured without dasatinib and with FITC-conjugated ODN2216 on ice were used as a negative control for endocytosis.

To observe translocation of TLR9 from ER to endosomes, pDCs were cultured in the absence or presence of 30 nM dasatinib for 1 h, and were stimulated with 0.5 μM ODN2216 without removing dasatinib for 2 h. ER-Tracker Red (Invitrogen, Carlsbad, CA) was added for 30 min before harvest. After fixation with 4% paraformaldehyde for 5 min at room temperature, permeabilization with 0.1% Triton X-100 for 5 min at −20°C, and blocking with 10% goat serum, the cells were stained with rabbit anti-EEA1 mAb (C45B10) or rabbit anti-Rab5 mAb (C8B1) (Cell Signaling Technology, Danvers, MA, USA) followed by Alexa Fluor 555-conjugated goat anti-rabbit IgG (Cell Signaling Technology), and were stained with biotinylated mouse anti-TLR9 mAb (26C593.2) (IMGENEX, San Diego, CA, USA) followed by Alexa Fluor 488-conjugated streptavidin (Invitrogen).

To observe nuclear translocation of IRF7 and NF-κB, pDCs were cultured in the absence or presence of 30 nM dasatinib for 1 h, and were stimulated with 0.5 μM ODN2216 without removing dasatinib for 3 h. After fixation with 2% paraformaldehyde for 15 min at 37°C, permeabilization with 100% methanol for 10 min at −20°C, and blocking with 10% goat serum, the cells were stained with rabbit anti-IRF7 (sc-9083) or NF-κBp65 (sc-109) polyclonal antibody (Santa Cruz Biotechnology, Santa Cruz, CA, USA) followed by Alexa Fluor 488-conjugated goat-anti rabbit IgG (Invitrogen). Nuclei were identified using TOTO-3 dye (Invitrogen).

To observe intracellular trafficking of CpG ODN, pDCs were cultured in the absence or presence of 30 nM dasatinib, 5 μM imatinib, 10 μM PP2, or 5 μM SU6656 for 1 h, and were incubated with 6 μM FITC-conjugated ODN2216 without removing the inhibitors for 90 min. After fixation with 4% paraformaldehyde for 5 min at room temperature, permeabilization with 0.1% Triton X-100 for 5 min at −20°C, and blocking with 10% goat serum, the cells were stained with anti-EEA1, anti-Rab5 mAb, or rabbit anti-Rab7 XP mAb (D95F2), followed by Alexa Fluor 555-conjugated goat anti-rabbit IgG (Cell Signaling Technology). Alternatively, the cells were stained with PE-conjugated mouse anti-LAMP-1 mAb (BioLegend) after blocking for 30 min using Image-iT FX signal enhancer (Invitrogen).

The cells were attached to slide glass by cytospin centrifuge and examined with an oil immersion objective (×60 Plan Apo, numerical aperture 1.4) by LSM510 META confocal microscope (Carl Zeiss, Oberkochen, Germany). Data were acquired with LMS5 software Version 3.2 (Carl Zeiss).

Colocalization analysis

Images were analyzed with Fiji (http://fiji.sc/wiki/index.php/Fiji), an image-processing package based on ImageJ. Colocalization amounts were analyzed using Manders' Colocalization Coefficients [21, 22] with the Costes' method of automatic thresholding [22, 23] using the Coloc_2 plug-in. The coefficient value represents the fraction of green in compartments containing red.

Statistical analyses

Data are presented as means ± SE. The significance of differences was determined by paired two-tailed *t*-test for cytokine and viability data and by Mann–Whitney *U*-test with Bonferroni correction following Kruskal–Wallis *H*-test for microscopy data. Difference with $p < 0.05$ was considered significant.

Acknowledgments: We thank Bristol-Myers Squibb Company for providing dasatinib, Novartis Phama for providing imatinib and nilotinib, Masaki Yasukawa for providing HSV-1, Reiko Saito for providing influenza virus, Keiko Fukunaga (Kyoto University) for her excellent technical assistance, Takashi Uchiyama (Kyoto University) for his supervision, the physicians who provided blood samples from patients treated with the TKIs, and Shin-ichiro Fujii (RIKEN, Research Center for Allergy and Immunology, Japan) for reviewing the manuscript. This study was supported by research funding from Ministry of Education, Culture, Sports, Science, and Technology of Japan (17016034) and from Japan Science and Technology Agency, Core Research for Evolutional Science and Technology (CREST) (to N.K.).

Conflict of Interest: The authors declare no financial or commercial conflict of interest.

References

1 Liu, Y.-J., IPC: professional type 1 interferon-producing cells and plasmacytoid dendritic cell precursors. *Annu. Rev. Immunol.* 2005. **23**: 275–306.

2 Gilliet, M., Cao, W. and Liu, Y.-J., Plasmacytoid dendritic cells: sensing nucleic acids in viral infection and autoimmune diseases. *Nat. Rev. Immunol.* 2008. **8**: 594–606.

3 Ganguly, D., Chamilos, G., Lande, R., Gregorio, J., Meller, S., Facchinetti, V., Homey, B. et al., Self-RNA-antimicrobial peptide complexes activate human dendritic cells through TLR7 and TLR8. *J. Exp. Med.* 2009. **206**: 1983–1994.

4 Weisberg, E., Manley, P. W., Cowan-Jacob, S. W., Hochhaus, A. and Griffin, J. D., Second generation inhibitors of BCR-ABL for the treatment of imatinib-resistant chronic myeloid leukaemia. *Nat. Rev. Cancer* 2007. **7**: 345–356.

5 Lombardo, L. J., Lee, F. Y., Chen, P., Norris, D., Barrish, J. C., Behnia, K., Castaneda, S. et al., Discovery of N-(2-chloro-6-methylphenyl)-2-(6-(4-(2-hydroxyethyl)- piperazin-1-yl)-2-methylpyrimidin-4-ylamino)thiazole-5-carboxamide (BMS-354825), a dual Src/Abl kinase inhibitor with potent antitumor activity in preclinical assays. *J. Med. Chem.* 2004. **47**: 6658–6661.

6 Schade, A. E., Schieven, G. L., Townsend, R., Jankowska, A. M., Susulic, V., Zhang, R., Szpurka, H. and Maciejewski, J. P., Dasatinib, a small-molecule protein tyrosine kinase inhibitor, inhibits T-cell activation and proliferation. *Blood* 2008. **111**: 1366–1377.

7 Fei, F., Yu, Y., Schmitt, A., Rojewski, M. T., Chen, B., Greiner, J., Götz, M. et al., Dasatinib exerts an immunosuppressive effect on CD8+ T cells specific for viral and leukemia antigens. *Exp. Hematol.* 2008. **36**: 1297–1308.

8 Blake, S. J., Bruce Lyons, A., Fraser, C. K., Hayball, J. D. and Hughes, T. P., Dasatinib suppresses in vitro natural killer cell cytotoxicity. *Blood* 2008. **111**: 4415–4416.

9 Salih, J., Hilpert, J., Placke, T., Grünebach, F., Steinle, A., Salih, H. R. and Krusch, M., The BCR/ABL-inhibitors imatinib, nilotinib and dasatinib differentially affect NK cell reactivity. *Int. J. Cancer* 2010. **127**: 2119–2128.

10 Manley, P. W., Stiefl, N., Cowan-Jacob, S. W., Kaufman, S., Mestan, J., Wartmann, M., Wiesmann, M. et al., Structural resemblances and comparisons of the relative pharmacological properties of imatinib and nilotinib. *Bioorg. Med. Chem.* 2010. **18**: 6977–6986.

11 Honda, K., Ohba, Y., Yanai, H., Negishi, H., Mizutani, T., Takaoka, A., Taya, C. and Taniguchi, T., Spatiotemporal regulation of MyD88-IRF-7 signalling for robust type-I interferon induction. *Nature* 2005. **434**: 1035–1040.

12 Guiducci, C., Ott, G., Chan, J. H., Damon, E., Calacsan, C., Matray, T., Lee, K.-D. et al., Properties regulating the nature of the plasmacytoid dendritic cell response to Toll-like receptor 9 activation. *J. Exp. Med.* 2006. **203**: 1999–2008.

13 Krieg, A. M., CpG motifs in bacterial DNA and their immune effects. *Annu. Rev. Immunol.* 2002. **20**: 709–760.

14 Kerkmann, M., Costa, L. T., Richter, C., Rothenfusser, S., Battiany, J., Hornung, V., Johnson, J. et al., Spontaneous formation of nucleic acid-based nanoparticles is responsible for high interferon-{alpha} induction by CpG-A in plasmacytoid dendritic cells. *J. Biol. Chem.* 2005. **280**: 8086–8093.

15 Lande, R., Gregorio, J., Facchinetti, V., Chatterjee, B., Wang, Y.-H., Homey, B., Cao, W. et al., Plasmacytoid dendritic cells sense self-DNA coupled with antimicrobial peptide. *Nature* 2007. **449**: 564–569.

16 Krug, A., Rothenfusser, S., Hornung, V., Jahrsdorfer, B., Blackwell, S., Ballas, Z. K., Endres, S. et al., Identification of CpG oligonucleotide sequences with high induction of IFN-alpha/beta in plasmacytoid dendritic cells. *Eur. J. Immunol.* 2001. **31**: 2154–2163.

17 Hanke, J. H., Gardner, J. P., Dow, R. L., Changelian, P. S., Brissette, W. H., Weringer, E. J., Pollok, B. A. and Connelly, P. A., Discovery of a novel, potent, and Src family-selective tyrosine kinase inhibitor. *J. Biol. Chem.* 1996. **271**: 695–701.

18 Blake, R. A., Broome, M. A., Liu, X., Wu, J., Gishizky, M., Sun, L. and Courtneidge, S. A., SU6656, a selective Src family kinase inhibitor, used to probe growth factor signaling. *Mol. Cell. Biol.* 2000. **20**: 9018–9027.

19 Latz, E., Schoenemeyer, A., Visintin, A., Fitzgerald, K. A., Monks, B. G., Knetter, C. F., Lien, E. et al., TLR9 signals after translocating from the ER to CpG DNA in the lysosome. *Nat. Immunol.* 2004. **5**: 190–198.

20 Hirai, M., Kadowaki, N., Kitawaki, T., Fujita, H., Takaori-Kondo, A., Fukui, R., Miyake, K. et al., Bortezomib suppresses function and survival of plasmacytoid dendritic cells by targeting intracellular trafficking of Toll-like receptors and endoplasmic reticulum homeostasis. *Blood* 2011. **117**: 500–509.

21 Manders, E. M. M., Verbeek, F. J. and Aten, J. A., Measurement of colocalization of objects in dual-color confocal images. *J. Microsc.* 1993. **169**: 375–382.

22 Dunn, K. W., Kamocka, M. M. and McDonald, J. H., A practical guide to evaluating colocalization in biological microscopy. *Am. J. Physiol. Cell Physiol.* 2011. **300**: C723-C742.

23 Costes, S. V., Daelemans, D., Cho, E. H., Dobbin, Z., Pavlakis, G. and Lockett, S., Automatic and quantitative measurement of protein-protein colocalization in live cells. *Biophys. J.* 2004. **86**: 3993–4003.

24 Kaisho, T. and Tanaka, T., Turning NF-[kappa]B and IRFs on and off in DC. *Trends Immunol.* 2008. **29**: 329–336.

25 Park, B., Brinkmann, M. M., Spooner, E., Lee, C. C., Kim, Y.-M. and Ploegh, H. L., Proteolytic cleavage in an endolysosomal compartment is required for activation of Toll-like receptor 9. *Nat. Immunol.* 2008. **9**: 1407–1414.

26 Maeda, T., Murata, K., Fukushima, T., Sugahara, K., Tsuruda, K., Anami, M., Onimaru, Y. et al., A novel plasmacytoid dendritic cell line, CAL-1, established from a patient with blastic natural killer cell lymphoma. *Int. J. Hematol.* 2005. **81**: 148–154.

27 Sanjuan, M. A., Rao, N., Lai, K.-T. A., Gu, Y., Sun, S., Fuchs, A., Fung-Leung, W.-P. et al., CpG-induced tyrosine phosphorylation occurs via a

TLR9-independent mechanism and is required for cytokine secretion. *J. Cell Biol.* 2006. **172**: 1057–1068.

28 **Liberali, P., Rämö, P. and Pelkmans, L.**, Protein kinases: starting a molecular systems view of endocytosis. *Annu. Rev. Cell Dev. Biol.* 2008. **24**: 501–523.

29 **Bantscheff, M., Eberhard, D., Abraham, Y., Bastuck, S., Boesche, M., Hobson, S., Mathieson, T. et al.**, Quantitative chemical proteomics reveals mechanisms of action of clinical ABL kinase inhibitors. *Nat. Biotechnol.* 2007. **25**: 1035–1044.

30 **Rix, U., Hantschel, O., Durnberger, G., Remsing Rix, L. L., Planyavsky, M., Fernbach, N. V., Kaupe, I. et al.**, Chemical proteomic profiles of the BCR-ABL inhibitors imatinib, nilotinib, and dasatinib reveal novel kinase and nonkinase targets. *Blood* 2007. **110**: 4055–4063.

31 **Karaman, M. W., Herrgard, S., Treiber, D. K., Gallant, P., Atteridge, C. E., Campbell, B. T., Chan, K. W. et al.**, A quantitative analysis of kinase inhibitor selectivity. *Nat. Biotechnol.* 2008. **26**: 127–132.

32 **Li, J., Rix, U., Fang, B., Bai, Y., Edwards, A., Colinge, J., Bennett, K. L. et al.**, A chemical and phosphoproteomic characterization of dasatinib action in lung cancer. *Nat. Chem. Biol.* 2010. **6**: 291–299.

33 **Sasai, M., Linehan, M. M. and Iwasaki, A.**, Bifurcation of Toll-Like receptor 9 signaling by adaptor protein 3. *Science* 2010. **329**: 1530–1534.

34 **Blasius, A. L., Arnold, C. N., Georgel, P., Rutschmann, S., Xia, Y., Lin, P., Ross, C. et al.**, Slc15a4, AP-3, and Hermansky-Pudlak syndrome proteins are required for Toll-like receptor signaling in plasmacytoid dendritic cells. *Proc. Natl. Acad. Sci. USA* 2010. **107**: 19973–19978.

35 **Lee, J., Tattoli, I., Wojtal, K. A., Vavricka, S. R., Philpott, D. J. and Girardin, S. E.**, pH-dependent internalization of muramyl peptides from early endosomes enables Nod1 and Nod2 signaling. *J. Biol. Chem.* 2009. **284**: 23818–23829.

36 **Di Pietro, S. M., Falcón-Pérez, J. M., Tenza, D., Setty, S. R. G., Marks, M. S., Raposo, G. and Dell'Angelica, E. C.**, BLOC-1 interacts with BLOC-2 and the AP-3 complex to facilitate protein trafficking on endosomes. *Mol. Biol. Cell* 2006. **17**: 4027–4038.

37 **Setty, S. R. G., Tenza, D., Truschel, S. T., Chou, E., Sviderskaya, E. V., Theos, A. C., Lamoreux, M. L. et al.**, BLOC-1 is required for cargo-specific sorting from vacuolar early endosomes toward lysosome-related organelles. *Mol. Biol. Cell* 2007. **18**: 768–780.

38 **Kawamura, K., Kadowaki, N., Kitawaki, T. and Uchiyama, T.**, Virus-stimulated plasmacytoid dendritic cells induce CD4 +cytotoxic regulatory T cells. *Blood* 2006. **107**: 1031–1038.

39 **Hartmann, G., Weeratna, R. D., Ballas, Z. K., Payette, P., Blackwell, S., Suparto, I., Rasmussen, W. L. et al.**, Delineation of a CpG phosphorothioate oligodeoxynucleotide for activating primate immune responses in vitro and in vivo. *J. Immunol.* 2000. **164**: 1617–1624.

Abbreviations: **ALL**: acute lymphoblastic leukemia · **AP**: adaptor protein · **BLOC**: biogenesis of lysosome-related organelles complex · **CML**: chronic myeloid leukemia · **DOTAP**: 1,2-dioleoyloxy-3-trimethylammonium-propane · **IRF**: IFN regulatory factor · **ODN**: oligodeoxynucleotide · **pDC**: plasmacytoid DC · **Ph**: Philadelphia · **SFK**: SRC family kinase · **TKI**: tyrosine kinase inhibitor

Full correspondence: Dr. Norimitsu Kadowaki, Department of Hematology and Oncology, Graduate School of Medicine, Kyoto University, 54 Shogoin Kawara-cho, Sakyo-ku, Kyoto 606-8507, Japan
Fax: +81-75-751-4963
e-mail: kadowaki@kuhp.kyoto-u.ac.jp

Received: 23/5/2012
Revised: 21/9/2012
Accepted: 24/10/2012
Accepted article online: 30/10/2012

AIDS RESEARCH AND HUMAN RETROVIRUSES
Volume 29, Number 6, 2013

DOI: 10.1089/aid.2012.0369

A Naturally Occurring Single Amino Acid Substitution in Human TRIM5α Linker Region Affects Its Anti-HIV Type 1 Activity and Susceptibility to HIV Type 1 Infection

Emi E. Nakayama,[1,*] Toshiaki Nakajima,[2,3,*] Gurvinder Kaur,[4] Jun-ich Mimaya,[5] Hiroshi Terunuma,[6] Narinder Mehra,[4] Akinori Kimura,[2,3] and Tatsuo Shioda[1]

Abstract

TRIM5α is a factor contributing to intracellular defense mechanisms against retrovirus infection. Rhesus and cynomolgus monkey TRIM5αs potently restrict HIV-1, whereas human TRIM5α shows weak effects against HIV-1. We investigated the association between a single nucleotide polymorphism in the TRIM5α linker 2 region (rs11038628), which substituted aspartic acid (D) for glycine (G) at position 249, with susceptibility to HIV-1 infection in Japanese and Indian subjects. rs11038628 is rare in Europeans but common in Asians and Africans. Functional analyses were performed by multiple-round replication and single-round assays, and indicated that the G249D substitution attenuated anti-HIV-1 activity of human TRIM5α. A slight attenuation of anti-HIV-2 activity was also observed in TRIM5α with 249D. The predicted secondary structure of the linker region suggested that the 249D substitution extended the α-helix in the neighboring coiled-coil domain, suggesting that human TRIM5α with 249D may lose the flexibility required for optimal recognition of retroviral capsid protein. We further analyzed the frequency of G249D in Japanese (93 HIV-1-infected subjects and 279 controls) and Indians (227 HIV-1-infected subjects and 280 controls). The frequency of 249D was significantly higher among HIV-1-infected Indian subjects than in ethnicity-matched control subjects [odds ratio (OR) = 1.52, $p = 0.026$]. A similar weak tendency was observed in Japanese subjects, but it was not statistically significant (OR = 1.19, $p = 0.302$). In conclusion, G249D, a common variant of human TRIM5α in Asians and Africans, is associated with increased susceptibility to HIV-1 infection.

Introduction

TRIM5α FROM RHESUS MONKEYS restricts human immunodeficiency virus-1 (HIV-1) replication at the postentry,[1] preintegration stage in the viral life cycle through rapid degradation of the HIV-1 core,[2] whereas human TRIM5α restricts HIV-1 only weakly but potently restricts N-tropic murine leukemia virus.[3,4] TRIM5α is a member of the tripartite motif-containing proteins and consists of RING, B-box 2, coiled-coil, and PRYSPRY (B30.2) domains. TRIM5α recognizes the multimerized capsid (CA) proteins of an incoming virus by its α-isoform-specific PRYSPRY domain. Studies of chimeric TRIM5αs have shown that the determinant of species-specific restriction against viral infection resides in the variable regions of the PRYSPRY domain.[5–11]

Infection by HIV-1 and progression to acquired immune deficiency syndrome (AIDS) vary among human individuals, and these phenomena are considered to be at least partially controlled by diversity in the human genome.[12,13] Two common TRIM5α functional polymorphisms, H43Y and R136Q, have been studied with regard to the association with HIV-1 infection.[14–21] Price *et al.* sequenced exon 2 of the *TRIM5* gene in 1,032 women enrolled in a long-term monitored Pumwani sex worker cohort, and found that women with the R136Q polymorphism were less likely to seroconvert despite heavy exposure to HIV-1 through active sex work.[15] Previous studies, including ours, showed the reduced antiviral activity of the H43Y substitution, but the associations with HIV-1 infection and disease progression were inconsistent among studies.[14,16–20] Javanbakht *et al.* reported a paradoxical

[1]Department of Viral Infections, Research Institute for Microbial Disease, Osaka University, Osaka, Japan.
[2]Department of Molecular Pathogenesis, Medical Research Institute, Tokyo Medical and Dental University, Tokyo, Japan.
[3]Laboratory of Genome Diversity, School of Biomedical Science, Tokyo Medical and Dental University, Tokyo, Japan.
[4]Department of Transplant Immunology and Immunogenetics, All India Institute of Medical Sciences, New Delhi, India.
[5]Division of Hematology and Oncology, Shizuoka Children's Hospital, Shizuoka, Japan.
[6]Biotherapy Institute of Japan, Tokyo, Japan.
*These authors contributed equally to this work.

protective effect of TRIM5α with 43Y against HIV-1 transmission in African-Americans.[14] Taken together, these findings indicate that anti-HIV-1 activity of human TRIM5α cannot protect humans from an HIV-1 pandemic, but may affect the rate of HIV-1 transmission.

In the present study, we investigated the association between a single nucleotide polymorphism (SNP) in the TRIM5α linker 2 region (rs11038628) between coiled-coil and PRYSPRY domains with susceptibility to HIV-1 infection. This SNP substituted aspartic acid (D) for glycine (G) at position 249. We show here that this SNP is associated with increased susceptibility to HIV-1 infection.

Materials and Methods

Cloning and expression of TRIM5α

The generation of recombinant Sendai viruses (SeVs) expressing human TRIM5α derived from MT4 cells, rhesus monkey TRIM5α derived from LLC-MK2 cells, and cynomolgus monkey TRIM5α lacking the PRYSPRY domain has been previously described.[9,22] All these TRIM5αs carried a hemagglutinin (HA) tag (YPYDVPDYAA) at the C-terminus. The D-to-G substitution at the 249th position was introduced into MT4 TRIM5α by polymerase chain reaction (PCR) site-directed mutagenesis. The resultant PCR fragment was cloned into pSeV18+b(+) as a vector. Recombinant SeVs expressing human TRIM5α carrying G at position 249 were recovered according to the previously described method.[23] The second passages in embryonated chicken eggs were used as stock virus for all experiments.

Western blotting analysis

MT4 cells (1×10^6) infected with recombinant SeVs expressing HA-tagged TRIM5α proteins were lysed in lysis buffer (50 mM Tris–HCl, pH 7.5, 150 mM NaCl, 1% Nonidet P40, 0.5% sodium deoxycholate). TRIM5α proteins in the lysates were subjected to sodium dodecyl sulfate-polyacrylamide gel electrophoresis (SDS-PAGE). Proteins in the gel were then electronically transferred onto a membrane (Immobilon; Millipore, Billerica, MA). Blots were blocked and probed with anti-HA high-affinity rat monoclonal antibody (Roche, Indianapolis, IN) overnight at 4°C. Blots were then incubated with peroxidase-conjugated anti-rat IgG (American Qualex, San Clemente, CA), and bound antibodies were visualized with a Chemilumi-One chemiluminescent kit (Nacalai Tesque, Kyoto, Japan).

Viral infection

MT4 cells (1×10^6) were infected with SeVs expressing MT4-derived human TRIM5α (249D), human TRIM5α (249G), rhesus monkey TRIM5α, or cynomolgus monkey TRIM5α lacking the PRYSPRY domain [CM-TRIM5α-SPRY(−)] at a multiplicity of infection (MOI) of 10 plaque-forming units (PFU) per cell and incubated at 37°C for 9 h. Aliquots of 1×10^5 cells were then superinfected with HIV-1 NL43 or HIV-2 GH123. Each superinfection used a titer of virus corresponding to 7 ng of p24 of NL43 or 20 ng of p25 of GH123. Experiments were performed with triplicate samples. The culture supernatants were collected periodically and the level of p24 or p25 was measured using a RETROtek antigen ELISA kit (ZeptoMetrix, Buffalo, NY). For the single-round infection assay, hamster TK-ts13 cells were infected with SeV expressing TRIM5α as described above, and superinfected with a vesicular stomatitis virus glycoprotein (VSV-G) pseudotyped HIV-1 vector expressing green fluorescence protein (GFP) under the control of the cytomegalovirus (CMV) promoter. The original HIV-1 vector was based on the BH10 strain.[24,25] To construct the lentivector possessing CA of NL4-3, we replaced the *Eco*RI–*Apa*I fragment corresponding to MA and CA of the pMDLg/p.RRE packaging vector with that of NL4-3.[26] In case of HIV-2, we used a canine cell line Cf2Th and VSV-G pseudotyped HIV-2 vector expressing GFP under the control of the LTR promoter.[27] Two days after infection, the cells were fixed with formaldehyde, and GFP-expressing cells were counted by a flow cytometer.

Human DNA subjects

The protocol for the present study was approved by the Ethics Review Board of the Medical Research Institute of Tokyo Medical and Dental University and that of the All India Institute of Medical Science. At setup of the cohort of HIV-1-infected Japanese subjects with hemophilia in 1995, all patients had been infected for longer than 10 years but were asymptomatic without any antiviral measures. Blood samples were collected from 93 well-characterized patients who were selected from the cohort after obtaining written informed consent.[28,29] Control DNA samples were prepared from Epstein–Barr virus-transformed human B cell lines established from randomly selected healthy donors ($n=279$) and obtained from the Japan Health Sciences Foundation. DNA samples from HIV-1-infected individuals were prepared from the blood samples using a QuickGene DNA whole blood kit S (Fujifilm, Tokyo, Japan). In addition, blood DNA samples were obtained from 227 HIV-1-infected Indian subjects and 226 healthy Indian volunteers with informed consent in related hospitals with the All India Institute of Medical Sciences, New Delhi.

Identification and genotyping of nucleotide variations in TRIM5α exon 5

Primer sets were designed to amplify the genomic segments covering the entire TRIM5α exon 5 as follows: sense primer (5′-GATGCGGTCATGCTATGTTG-3′) and antisense primer (5′-CGAATGCTGATTTATGACCATA-3′). Genomic DNA was subjected to PCR amplification followed by sequencing using a BigDye Terminator v3.1 Cycle Sequencing Kit (Applied Biosystems, Foster City, CA). Polymorphisms were identified using the Sequencher program (Gene Code Co., Ann Arbor, MI).

Statistical analysis

All statistical analyses in this study were performed using GraphPad InStat version 3.06 for Windows (GraphPad Software, San Diego, CA). Pairwise linkage disequilibrium (LD) (r^2) was estimated using SNPAlyze version 6.0 standard (Dynacom Co., Ltd., Chiba, Japan).

Prediction of the peptide secondary structure

The Chou–Fasman methods were used to predict the secondary structure of TRIM5α using GENETYX-MAC version 15 software (Genetyx Corporation, Tokyo, Japan).

Results

Anti-HIV-1 activity of TRIM5α was attenuated by G249D substitution

We previously cloned human TRIM5α from the CD4-positive T cell line MT4 and noted that there is a G-to-D amino acid substitution (G249D) in comparison with the reference sequence (NM_033034).[9] This position is known as a polymorphic site in the human *TRIM5* gene (rs11038628) located in the linker 2 region between the coiled-coil and PRYSPRY domains (Fig. 1). Initially, we speculated that this polymorphism would have no effect on antiviral activity due to its presence in the linker 2 region. Goldschmidt *et al.*[18] reported that HeLa cells stably transduced with TRIM5α with 249D did not differ in susceptibility to HIV-1 infection. However, a tendency toward higher *in vitro* p24 production was observed at 7 days after infection in peripheral blood mononuclear cells from white subjects with the 249D allele, although the difference was not statistically significant mainly due to the limited number of subjects with the mutant allele.[18] In addition, Old World monkey TRIM5α, including those of African green monkey, rhesus monkey, and cynomolgus monkey, also bears G at this position (Fig. 1). The HapMap project showed the 249D allele to be rare in whites (allele frequency: 0.053) but common in Japanese (allele frequency: 0.343) and African populations (allele frequency: 0.367). These findings prompted us to reevaluate the effects of this SNP on HIV-1 infection in Asians in which the frequency of G249D is higher than in whites.

To investigate the functional significance of G249D on the anti-HIV activity of TRIM5α, we constructed SeV containing C-terminal HA-tagged human TRIM5α (249G) (Fig. 1) by site-directed mutagenesis on MT4 TRIM5α, which bears D at position 249. As shown in Fig. 2A, the expression level of TRIM5α (249G) was comparable to that of TRIM5α (249D) in recombinant SeV-infected MT4 cells.

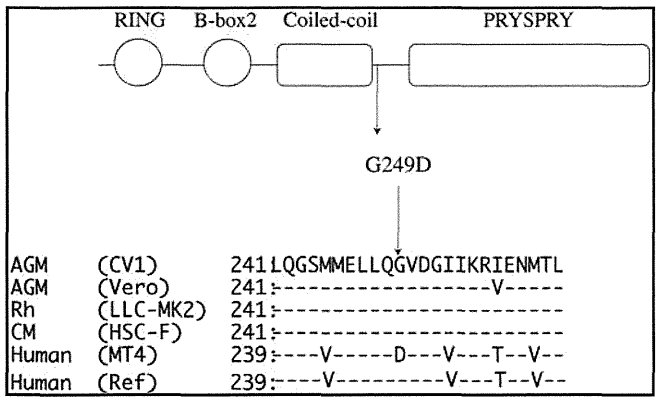

FIG. 1. Schematic presentation of TRIM5α structure. Circles and squares represent functional domains of TRIM5α. The position of the G249D polymorphism is shown by arrows. The amino acid sequences of African green monkey (AGM) TRIM5α from CV1[9] and Vero cells, rhesus monkey (Rh) TRIM5α from LLC-MK2,[10] cynomolgus monkey (CM) TRIM5α from HSC-F,[9] human TRIM5α from MT4 cells,[9] and the reference sequence (NM_033034) were aligned. Dashes denote an identical amino acid to AGM TRIM5α from CV1.

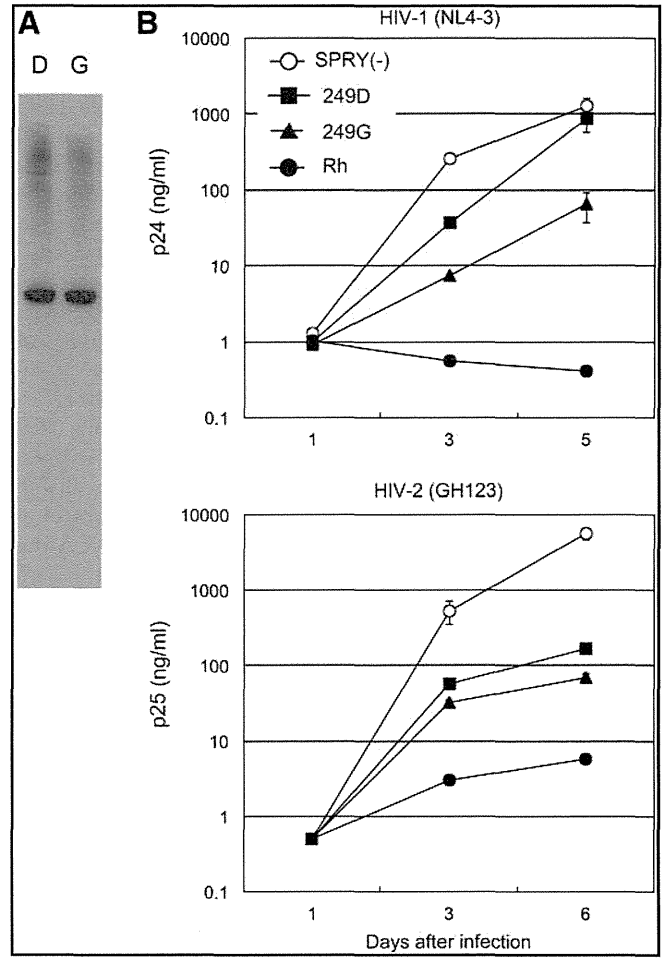

FIG. 2. **(A)** Lysates of MT4 cells infected with recombinant Sendai virus (SeV) expressing hemagglutinin (HA)-tagged human TRIM5α with 249D (lane D) and with 249G (lane G) were visualized by western blotting with an antibody against HA. Representative results of three independent experiments are shown. **(B)** MT4 cells were infected with SeV expressing TRIM5α lacking the PRYSPRY domain [SPRY(−); white circles], MT4-derived human TRIM5α (249D; black squares), human TRIM5α (249G; black triangles), or rhesus monkey TRIM5α (Rh; black circles). Nine hours after SeV infection, cells were inoculated with HIV-1 strain NL4-3 or HIV-2 strain GH123, and culture supernatants were periodically assayed for levels of p24 or p25, respectively. Data points are means for triplicate samples with SD. Three and six days after infection, statistically significant differences ($p < 0.05$) of HIV-1 and HIV-2 growth were observed between human TRIM5α (249D) and human TRIM5α (249G) by unpaired *t* test. Representative data of at least three independent experiments are shown.

These TRIM5α constructs were tested for their ability to restrict the X4-tropic HIV-1 strain NL4-3 and HIV-2 strain GH123. MT4 cells infected with recombinant SeV expressing each of the TRIM5α constructs were superinfected with HIV-1 NL4-3 or HIV-2 GH123. We used SeV expressing cynomolgus monkey TRIM5α lacking the PRYSPRY domain as a negative control for functional TRIM5α, as overexpression of TRIM5α lacking the PRYSPRY domain was shown to exert a dominant negative effect on endogenous human TRIM5α.[30] As shown in Fig. 2B, MT4-derived human TRIM5α (249D) showed only

weak anti-HIV-1 activity, as we demonstrated previously.[21] On the other hand, human TRIM5α (249G) showed stronger restriction activity to HIV-1 NL4-3 than human TRIM5α (249D). In the case of HIV-2, both human TRIM5α with 249G and 249D exhibited apparent anti-HIV-2 activity. The human TRIM5α (249G) showed stronger restriction activity to HIV-2 GH123 than human TRIM5α (249D), although the difference was very small (Fig. 2B, lower panel). These results indicated that the G249D variant weakened the anti-HIV-1 and anti-HIV-2 activities of human TRIM5α.

TRIM5α is known to restrict viral infection at the early steps of HIV replication. To evaluate the anti-HIV-1 activity of human TRIM5α at the early stages, we performed the single-round infection assay using a GFP expression vector (Fig. 3). The hamster cell line TK-ts13, which lacks endogenous TRIM5α expression, was infected with recombinant SeV expressing human TRIM5α. We superinfected cells with VSV-G pseudotyped lentivector expressing GFP under the control of the CMV promoter. We used HIV-1 vectors bearing CA derived from BH10 (Fig. 3A) and NL4-3 (Fig. 3B). Both HIV-1 GFP vectors were suppressed to a greater degree by human TRIM5α (249G) than by MT4-derived human TRIM5α (249D). A similar result was obtained when we used the HIV-2 GFP vector (Fig. 3C). Taken together, these observations indicated that the G249D polymorphism affected the anti-HIV-1 and anti-HIV-2 activities of human TRIM5α.

Associations of TRIM5α G249D polymorphism with susceptibility to HIV-1 infection

We sequenced TRIM5α exon 5 and found G249D in the populations tested. The associations of G249D polymorphism with susceptibility to HIV-1 infection are summarized in Table 1. The frequency of 249D was significantly higher in the HIV-1-infected Indian subjects than in the ethnicity-matched controls [odds ratio (OR) = 1.52, $p = 0.026$]. A similar tendency was also observed in the Japanese population, but did not reach statistical significance (OR = 1.19, $p = 0.302$).

Previously, we sequenced TRIM5α exons 2 of the same subjects as above and reported the association of H43Y with susceptibility to HIV-1 infection.[21] The levels of LD indicated that G249D in exon 5 and H43Y in exon 2 were not in tight linkage disequilibrium in either Japanese ($r^2 = 0.18$, $n = 188$) or Indian ($r^2 = 0.02$, $n = 96$) populations.

Discussion

The G249D polymorphism in TRIM5α is common in Asian and African populations. It was initially speculated that there was no functional effect of this SNP, as it is located outside of any functional domains of human TRIM5α. Contrary to our expectation, however, we observed attenuation of anti-HIV-1 and anti-HIV-2 activity of the G-for-D substitution with both multiround replication and single-round infection assays. Furthermore, we investigated two ethnic populations, Japanese and Indian, for the G249D polymorphism and found the association of the TRIM5α 249D allele with enhanced susceptibility to HIV-1 infection.

Amino acid position 249 of human TRIM5α lies within the linker region for which no three-dimensional structural data have yet been reported. Therefore, we performed secondary structure prediction by the Chou–Fasman method[31] to examine the possible effect of this SNP on the protein structure.

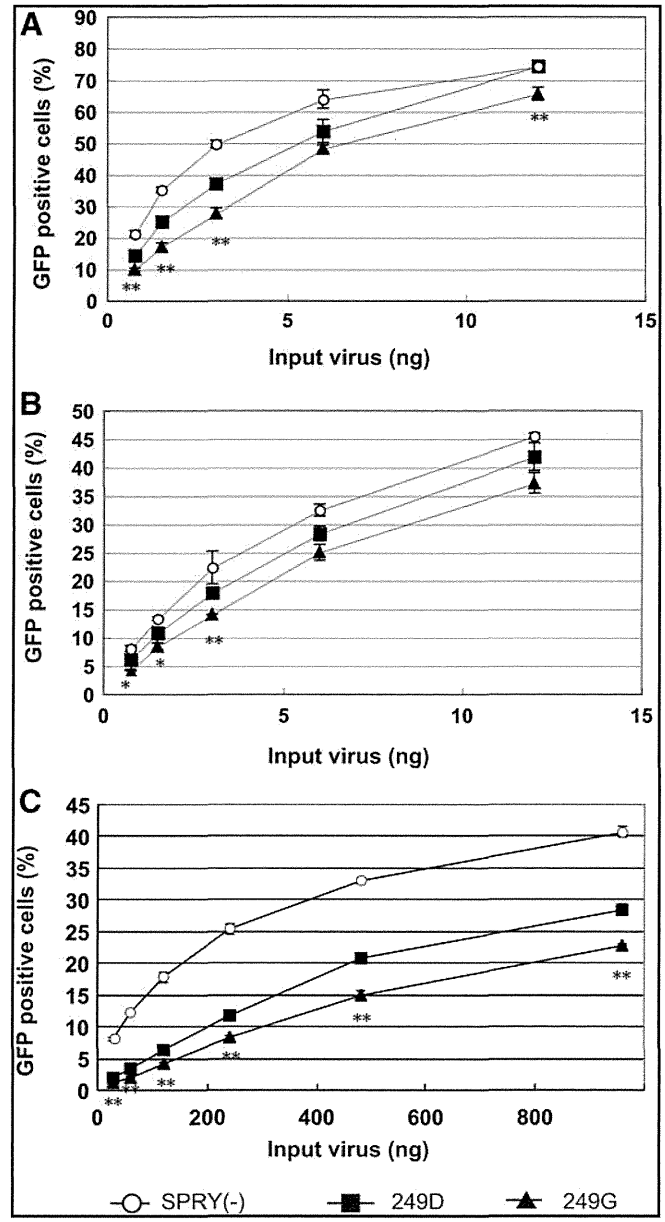

FIG. 3. TK-ts13 cells infected with SeVs expressing TRIM5α lacking the PRYSPRY domain [SPRY(−); white circles], MT4-derived human TRIM5α (249D; black squares), or human TRIM5α (249G; black triangles) were exposed to green fluorescence protein (GFP)-expressing HIV-1 vector based on BH10 **(A)** or NL4-3 **(B)**. **(C)** Cf2Th cells infected with SeVs were exposed to an HIV-2 vector based on ROD. GFP-positive cells were counted by a flow cytometer. Data points are means for triplicate samples with SD. *,** The statistically significant differences, $p < 0.05$ and $p < 0.001$, respectively, in unpaired t test between human TRIM5α (249D) and human TRIM5α (249G). Representative results of two independent experiments are shown.

The G-to-D substitution increased the probability of α-helix formation and resulted in the extension of the α-helix from the coiled-coil region into the linker 2 region. Similar results were obtained by the PREDETOR in http://mobyle.pasteur.fr (data not shown). This suggested that TRIM5α with 249G would be more flexible than TRIM5α with 249D.

TABLE 1. ASSOCIATION OF rs10038628 (G249D) WITH SUSCEPTIBILITY TO HIV-1 INFECTION IN JAPANESE AND INDIAN POPULATIONS

	Japanese				*Indian*			
	HIV-1-infected (n=93)	*Control* (n=279)	*Odds ratio* (95% CI)	p-*value*	*HIV-1-infected* (n=227)	*Control* (n=280)	*Odds ratio* (95% CI)	p-*value*
rs10038628								
GG	28 (30%)	98 (35%)	0.80 (0.48–1.32)	0.376	161 (71%)	226 (81%)	0.58 (0.39–0.88)	0.010
DG	47 (51%)	137 (49%)			63 (28%)	49 (17%)		
DD	18 (19%)	44 (16%)	1.28 (0.70–2.35)	0.422	3 (1%)	5 (2%)	0.74 (0.17–3.12)	0.736[a]
Allele D	83 (45%)	225 (40%)	1.19 (0.85–1.67)	0.302	69 (15%)	59 (11%)	1.52 (1.05–2.21)	0.026

[a]Fisher's exact test.

Human TRIM5α was obviously not effective in protecting against HIV-1 infection compared with the strong Old World monkey TRIM5α, as only humans are susceptible and Old World monkeys are resistant to HIV-1 infection. With experimental overexpression of human TRIM5α, the anti-HIV-1 activity of human TRIM5α was variable among previous reports.[1,5,9,14,16,20,21] Our previous data showed the weakest anti-HIV-1 activity of human TRIM5α,[9,20,21] even though we used the SeV system, which allowed high expression levels of inserted genes. As described in the present study, the 249D substitution would explain why our human TRIM5α derived from MT4 showed little potency against HIV-1. We examined the G249D SNP in commonly used human cell lines, CEM, HeLa, Jurkat, and 293T, and found that these were all homozygous for 249G, but MT4 was homozygous for 249D. This is not surprising because the allele frequency of 249D is high in Japan but quite rare in whites and MT4 cells were established from Japanese donor blood.[32] On the other hand, MT4 is highly susceptible to HIV-1 infection,[33] which is in good agreement with the present data.

Previously, Goldschmidt *et al.* failed to observe the attenuation of antiviral activity by the 249D mutation.[18] One possible reason for the discrepancy between their results and ours is the difference in expression system used. Goldschmidt *et al.* used HeLa cells stably transduced with TRIM5α with various mutations.[18] Transduced cell lines sometimes develop unexpected phenotypic changes during the cloning procedure. In contrast, we used the SeV system, and the conditions of cells infected with different recombinant viruses were always comparable, especially among those expressing full-length TRIM5α. It should be noted that Goldschmidt *et al.* also reported a tendency toward higher *in vitro* p24 production 7 days after infection in peripheral blood mononuclear cells from individuals with the 249D allele, which is consistent with our present results.[18]

We clearly showed that the 249D allele was associated with increased susceptibility to HIV-1 infection in the Indian population. However, although a similar tendency was observed in the Japanese population, the association was not significant. The precise reason why the effect of G249D was unclear in the Japanese population is not yet clear. It should be noted that our Japanese patients were infected through contaminated blood products in the early 1980s. On the other hand, the Indian patients were infected through heterosexual contact after the HIV-1 pandemic in Asia after 1990. It is possible that the difference in route of HIV-1 transmission may be responsible for this difference between Japanese and Indian patients. Further studies in well-characterized cohorts are necessary to confirm our findings regarding HIV-1 transmission and the possible effects of this SNP on AIDS progression.

Acknowledgments

We thank Ms. Setsuko Bando and Ms. Noriko Teramoto for their assistance, and Dr. Hirotaka Ode for critical suggestion. This work was supported by grants from the Ministry of Education, Culture, Sports, Science, and Technology, and the Ministry of Health, Labour, and Welfare, Japan.

Author Disclosure Statement

No competing financial interests exist.

References

1. Stremlau M, Owens CM, Perron MJ, Kiessling M, Autissier P, and Sodroski J: The cytoplasmic body component TRIM5alpha restricts HIV-1 infection in Old World monkeys. Nature 2004;427:848–853.
2. Stremlau M, Perron M, Lee M, *et al.*: Specific recognition and accelerated uncoating of retroviral capsids by the TRIM5alpha restriction factor. Proc Natl Acad Sci USA 2006;103:5514–5519.
3. Perron MJ, Stremlau M, Song B, Ulm W, Mulligan RC, and Sodroski J: TRIM5alpha mediates the postentry block to N-tropic murine leukemia viruses in human cells. Proc Natl Acad Sci USA 2004;101:11827–11832.
4. Yap MW, Nisole S, Lynch C, and Stoye JP: Trim5alpha protein restricts both HIV-1 and murine leukemia virus. Proc Natl Acad Sci USA 2004;101:10786–10791.
5. Perez-Caballero D, Hatziioannou T, Yang A, Cowan S, and Bieniasz PD: Human tripartite motif 5alpha domains responsible for retrovirus restriction activity and specificity. J Virol 2005;79:8969–8978.
6. Sawyer SL, Wu LI, Emerman M, and Malik HS: Positive selection of primate TRIM5alpha identifies a critical species-specific retroviral restriction domain. Proc Natl Acad Sci USA 2005;102:2832–2837.
7. Stremlau M, Perron M, Welikala S, and Sodroski J: Species-specific variation in the B30.2(SPRY) domain of TRIM5alpha determines the potency of human immunodeficiency virus restriction. J Virol 2005;79:3139–3145.
8. Yap MW, Nisole S, and Stoye JP: A single amino acid change in the SPRY domain of human Trim5alpha leads to HIV-1 restriction. Curr Biol 2005;15:73–78.

9. Nakayama EE, Miyoshi H, Nagai Y, and Shioda T: A specific region of 37 amino acid residues in the SPRY (B30.2) domain of African green monkey TRIM5alpha determines species-specific restriction of simian immunodeficiency virus SIVmac infection. J Virol 2005;79:8870–8877.
10. Kono K, Song H, Shingai Y, Shioda T, and Nakayama EE: Comparison of anti-viral activity of rhesus monkey and cynomolgus monkey TRIM5alphas against human immunodeficiency virus type 2 infection. Virology 2008;373: 447–456.
11. Perron MJ, Stremlau M, and Sodroski J: Two surface-exposed elements of the B30.2/SPRY domain as potency determinants of N-tropic murine leukemia virus restriction by human TRIM5alpha. J Virol 2006;80:5631–5636.
12. O'Brien SJ and Nelson GW: Human genes that limit AIDS. Nat Genet 2004;36:565–574.
13. Shioda T and Nakayama EE: Human genetic polymorphisms affecting HIV-1 diseases. Int J Hematol 2006;84:12–17.
14. Javanbakht H, An P, Gold B, *et al.*: Effects of human TRIM5alpha polymorphisms on antiretroviral function and susceptibility to human immunodeficiency virus infection. Virology 2006;354:15–27.
15. Price H, Lacap P, Tuff J, *et al.*: A TRIM5alpha exon 2 polymorphism is associated with protection from HIV-1 infection in the Pumwani sex worker cohort. AIDS 2010;24: 1813–1821.
16. Sawyer SL, Wu LI, Akey JM, Emerman M, and Malik HS: High-frequency persistence of an impaired allele of the retroviral defense gene TRIM5alpha in humans. Curr Biol 2006;16:95–100.
17. Speelmon EC, Livingston-Rosanoff D, Li SS, *et al.*: Genetic association of the antiviral restriction factor TRIM5alpha with human immunodeficiency virus type 1 infection. J Virol 2006;80:2463–2471.
18. Goldschmidt V, Bleiber G, May M, Martinez R, Ortiz M, and Telenti A: Role of common human TRIM5alpha variants in HIV-1 disease progression. Retrovirology 2006;3:54.
19. van Manen D, Rits MA, Beugeling C, van Dort K, Schuitemaker H, and Kootstra NA: The effect of Trim5 polymorphisms on the clinical course of HIV-1 infection. PLoS Pathog 2008;4:e18.
20. Nakayama EE, Carpentier W, Costagliola D, *et al.*: Wild type and H43Y variant of human TRIM5alpha show similar anti-human immunodeficiency virus type 1 activity both in vivo and in vitro. Immunogenetics 2007;59:511–515.
21. Nakajima T, Nakayama EE, Kaur G, *et al.*: Impact of novel TRIM5alpha variants, Gly110Arg and G176del, on the anti-HIV-1 activity and the susceptibility to HIV-1 infection. AIDS 2009;23:2091–2100.
22. Song H, Nakayama EE, Yokoyama M, Sato H, Levy JA, and Shioda T: A single amino acid of the human immunodeficiency virus type 2 capsid affects its replication in the presence of cynomolgus monkey and human TRIM5alphas. J Virol 2007;81:7280–7285.
23. Nakayama EE, Tanaka Y, Nagai Y, Iwamoto A, and Shioda T: A CCR2-V64I polymorphism affects stability of CCR2A isoform. AIDS 2004;18:729–738.
24. Miyoshi H, Takahashi M, Gage FH, and Verma IM: Stable and efficient gene transfer into the retina using an HIV-based lentiviral vector. Proc Natl Acad Sci USA 1997;94: 10319–10323.
25. Miyoshi H, Blomer U, Takahashi M, Gage FH, and Verma IM: Development of a self-inactivating lentivirus vector. J Virol 1998;72:8150–8157.
26. Kuroishi A, Bozek K, Shioda T, and Nakayama EE: A single amino acid substitution of the human immunodeficiency virus type 1 capsid protein affects viral sensitivity to TRIM5 alpha. Retrovirology 2010;7:58.
27. Miyamoto T, Nakayama EE, Yokoyama M, *et al.*: The carboxyl-terminus of human immunodeficiency virus type 2 circulating recombinant form 01_AB capsid protein affects sensitivity to human TRIM5alpha. PLoS One 2012;7:e47757.
28. Munkanta M, Terunuma H, Takahashi M, *et al.*: HLA-B polymorphism in Japanese HIV-1-infected long-term surviving hemophiliacs. Viral Immunol 2005;18:500–505.
29. Nakajima T, Ohtani H, Naruse T, *et al.*: Copy number variations of CCL3L1 and long-term prognosis of HIV-1 infection in asymptomatic HIV-infected Japanese with hemophilia. Immunogenetics 2007;59:793–798.
30. Maegawa H, Nakayama EE, Kuroishi A, and Shioda T: Silencing of tripartite motif protein (TRIM) 5alpha mediated anti-HIV-1 activity by truncated mutant of TRIM5alpha. J Virol Methods 2008;151:249–256.
31. Chou PY and Fasman GD: Prediction of the secondary structure of proteins from their amino acid sequence. Adv Enzymol Relat Areas Mol Biol 1978;47:45–48.
32. Akagi T, Ohtsuki Y, Shiraishi Y, and Miyoshi I: Transformation of human fetal thymus and spleen lymphocytes by human T-cell leukemia virus type I. Acta Med Okayama 1985;39:155–159.
33. Harada S, Koyanagi Y, and Yamamoto N: Infection of HTLV-III/LAV in HTLV-I-carrying cells MT-2 and MT-4 and application in a plaque assay. Science 1985;229:563–566.

Address correspondence to:
Tatsuo Shioda
Department of Viral Infections
Research Institute for Microbial Disease
Osaka University
3-1, Yamada-oka, Suita-shi
Osaka 565-0871 Japan

E-mail: shioda@biken.osaka-u.ac.jp

Journal of Autoimmunity 47 (2013) 25–33

Contents lists available at ScienceDirect

Journal of Autoimmunity

journal homepage: www.elsevier.com/locate/jautimm

A novel link of *HLA* locus to the regulation of immunity and infection: *NFKBIL1* regulates alternative splicing of human immune-related genes and influenza virus *M* gene

Jianbo An, Toshiaki Nakajima, Hiroki Shibata, Takuro Arimura, Michio Yasunami, Akinori Kimura*

Department of Molecular Pathogenesis, Medical Research Institute, Tokyo Medical and Dental University, Tokyo, Japan

ARTICLE INFO

Article history:
Received 28 June 2013
Received in revised form
19 July 2013
Accepted 27 July 2013

Keywords:
Alternative splicing
ASF/SF2
CLK1
Immune-related gene
NFKBIL1

ABSTRACT

HLA locus contains immune-related genes and genetically regulates immune responses against both foreign- and self-antigens in humans. Inhibitor of κB-like protein (IκBL), encoded by *HLA*-linked *NFKBIL1*, is a protein of unknown function, while genetic variations in *NFKBIL1* are known to associate with the susceptibility to inflammatory and/or autoimmune diseases. In this study, we found that IκBL suppressed exon exclusion in alternative splicing of human immune-related genes such as *CD45*. Yeast-two-hybrid screening and immunoprecipitation assay revealed molecular association of IκBL with CLK1, a serine/threonine and tyrosine kinase, which plays a role in the alternative splicing. Unexpectedly, we found that the regulation of alternative splicing in *CD45* by IκBL was independent from the kinase activity of CLK1. On the other hand, it was demonstrated that an SR protein, ASF/SF2, bound both IκBL and CLK1 at the RNA-recognition motifs of ASF/SF2, implying a competition of IκBL and CLK1 on SR protein. In addition, IκBL was found to regulate the CLK1-dependent synthesis of *M2* RNA, a splice variant of influenza A virus *M* gene. These observations suggest a functional involvement of IκBL in the regulation of alternative splicing in both human and viral genes, which is a novel link of *HLA* locus to the regulation of immunity and infection in humans.

1. Introduction

Human NF-κB inhibitor-like protein 1 gene (*NFKBIL1*) is located in the *HLA* class III region on the short arm of chromosome 6 and encodes a protein, inhibitor of κB-like protein (IκBL), which shows a limited homology to inhibitor of κB (IκB). A number of studies have demonstrated the association between genetic variations in *NFKBIL1* and susceptibility to inflammatory and/or autoimmune diseases, such as multiple sclerosis [1], rheumatoid arthritis (RA) [2], type I diabetes mellitus [3], Takayasu's arteritis [4], and chronic thromboembolic pulmonary hypertension [5]. It has been reported that the sequence variations in the promoter region of *NFKBIL1*, which showed the lowest and the highest promoter activity, would confer the susceptibility to RA and Takayasu's arteritis, respectively [4], implying that the altered expression of IκBL might contribute to the pathogenesis of immune-related diseases.

Alternative splicing is a crucial mechanism in the post-transcriptional control of gene expression in eukaryotes, in which target exons in pre-mRNA could be either excluded or included depending on the specific *cis*-regulatory elements and recognition by the splicing-related factors [6,7]. Pre-mRNAs of human immune-related genes are known to undergo extensive alternative splicing [8]. For example, resting T cells express larger mRNA isoforms of *CD45*, while target exons of *CD45* were selectively excluded to form shorter mRNA isoforms in activated T cells. Expression of each isoform generated by the alternative splicing is strictly regulated, whereas the abnormal alternative splicing events, which lead to altered expression of target mRNA isoforms, have been reported to associate with autoimmune diseases [9,10].

IκBL possesses nuclear localization sequences (NLS) at its N-terminus and localized in nuclear speckles [11,12], which are sub-nuclear structures enriched with pre-mRNA splicing factors [13]. In addition, IκBL was reported to associate with RNA [12]. These lines of evidence suggest that IκBL might play a role in the RNA splicing. In addition, it has been reported that CDC-like kinase 1 (CLK1),

* Corresponding author. Department of Molecular Pathogenesis, Medical Research Institute, Tokyo Medical and Dental University, 1-5-45 Yushima, Bunkyo-ku, Tokyo 113-8510, Japan. Tel.: +81 3 5803 4905; fax: +81 3 5803 4907.
E-mail address: akitis@mri.tmd.ac.jp (A. Kimura).

0896-8411/$ – see front matter © 2013 Elsevier Ltd. All rights reserved.
http://dx.doi.org/10.1016/j.jaut.2013.07.010

a serine/threonine and tyrosine kinase, localizes in nuclear speckles and nucleoplasm, and CLK1 regulates alternative splicing through phosphorylation of serine/arginine rich (SR) proteins [14–16]. SR proteins play an important role in both constitutive splicing and alternative splicing of pre-mRNA [6,7]. Functional domain of SR proteins contains one or two RNA-recognition motifs (RRMs), where pre-mRNAs were bound to be processed.

We report here that IκBL physically interacts with CLK1 and SR protein, and functions as a novel regulator in the alternative splicing of both human and viral genes.

2. Materials and methods

2.1. Calculation of Ka/Ks value for amino acid substitution

Ka/Ks value was used to estimate the potential functional domain of IκBL. The Ka and the Ks values are calculated by DnaSP v3.0 [17], by comparing the human and murine *NFKBIL1* sequences. Ks is the number of synonymous substitutions per synonymous site, whereas Ka is the number of nonsynonymous substitutions per nonsynonymous site.

2.2. Plasmids

An exon trapping vector, pSPL3 (Invitrogen, Carlsbad, CA, USA), was used to construct mini-genes analyzed for the alternative splicing. A *CD45* mini-gene construct covered exons 3–7 and their intron–exon boundary segments from human *CD45*, while *CD72* and *CTLA4* mini-gene constructs encompassed exons 7–8, and exons 2–4, respectively, with their intron–exon boundary segments from human the genes. We cloned human cDNAs encoding IκBL, CLK1, hnRNPLL, hnRNPL, FOX1 and ASF/SF2 into mammalian expression vectors, pCI-neo (Promega, Madison, WI, USA) and pEGFP (Clontech, Mountain View, CA, USA). Deletion mutants of IκBL (IκBL-ΔN, -ΔA, -ΔCv and -ΔCc), CLK1 (CLK1-ΔN, -Δkinase) and ASF/SF2 (ASF/SF2-ΔRRM1β1, -ΔRRM2β1, -ΔRRM1&2β1 and -ΔRS) were generated by the standard PCR-based method. All constructs were sequenced to ensure that undesired mutations were not introduced during the cloning procedure. The constructs used in the plasmid-based rescue system for the influenza A virus, including pPOLI-M-RT, pcDNA-NP, pcDNA-PB1, pcDNA-PB2 and pcDNA-PA, were kindly provided by Dr. George G. Brownlee and Dr. Ervin Fodor. Plasmid DNAs for transfection were prepared using QIAprep Spin Miniprep kit (Qiagen, Hilden, Germany).

2.3. Cell culture and transfection

COS7, HeLa and HEK293T cells (ATCC, Manassas, VA, USA) were maintained in Dulbecco's modified Eagle's medium (DMEM) (Invitrogen) supplemented with 10% de-complemented fetal calf serum (FCS) (Nichirei Biosciences, Tokyo, Japan) and Penicillin–Streptomycin–Glutamine (PSG) (Invitrogen). JSL1 cells were kindly provided by Dr. Kristen W. Lynch and maintained in RPMI1640 (Sigma, St. Louis, MO, USA) supplemented with 5% FCS plus PSG. Transfection was done using COSFectin (Bio-Rad, Hercules, CA, USA) or Lipofectamine2000 (Invitrogen), according to the manufacturer's instructions. Hygromycin (Invitrogen) was used for selection of a stably transfected JSL1 line, JSL-IκBL.

2.4. RNA interference

Knockdown of endogenous *NFKBIL1* and *CLK1* was done by using pre-designed siRNAs (siRNA ID for *NFKBIL1*: s9517 and s194653; siRNA ID for *CLK1*: s3162 and s3163) (Ambion, Austin, TX, USA). A non-targeting siRNA was used as a negative control.

2.5. Immunofluorescence staining

Fixed and permeabilized HeLa cells were incubated with anti-SC35 (BD Biosciences Pharmingen, San Diego, CA, USA) and/or anti-CLK1 (Abcam, Cambridge, MA, USA) antibodies, followed by incubation with fluorescence-conjugated second antibodies. Images were analyzed with an LSM510 laser-scanning microscope (Carl Zeiss, Oberkochen, Germany).

2.6. RNA isolation, RT-PCR and real-time RT-PCR

Total cellular RNAs from human tissues were purchased from Agilent Technologies. Total RNAs from cells were purified by using RNeasy Mini kit (Qiagen) and cDNAs were synthesized by the reverse transcription (RT) reaction from 1 μg of RNA using PrimeScript RT reagent Kit (Takara Bio, Tokyo, Japan) according to the manufacturer's protocol. To evaluate the amount of splicing variants, cDNA was applied to PCR and the PCR products were separated by electrophoresis on agarose gels, visualized by ethidium bromide staining, and quantified by using ImageJ Version 1.36. The endogenous expression of mRNA was quantified by real-time RT-PCR using iCycler iQ Real-Time PCR Detection System (Bio-Rad).

2.7. Yeast-two-hybrid (Y2H) screening

All procedures for Y2H were performed according to the manufacturer's instructions for the Matchmaker GAL4 Two-Hybrid System 3 (Clontech).

2.8. Immunoprecipitation (IP) and immunoblotting

IP products were prepared by precipitation of antigen–antibody complex using Protein G Sepharose beads (GE Healthcare, Uppsala, Sweden). For immunoblotting, samples were separated on a 10% SDS-PAGE gel and transferred to a nitrocellulose membrane (Invitrogen). After the incubation with antibodies, signals were visualized by Image Reader LAS-3000 (FUJIFILM, Tokyo, Japan).

2.9. Flow cytometry analysis

JSL1 and JSL1-IκBL cells with or without activation by 12-myristate 13-acetate (PMA) (Calbiochem, San Diego, CA, USA) were incubated with specific antibodies to CD45RA (eBioscience, San Diego, CA, USA) or CD45RO (Santa Cruz Biotechnology, Santa Cruz, CA, USA). Flow cytometry analysis was performed on FACS-Calibur (BD Biosciences, San Jose, CA, USA) according to the standard protocol.

2.10. Statistical analysis

Statistical comparisons were performed using Student's *t*-tests or one-way ANOVA followed by a post-hoc Bonferroni's or Dunnett's multiple comparison tests. The results were considered statistically significant when the p value was less than 0.05.

Additional information to *2.4.*, *2.5.*, *2.7.*, *2.8.* and antibodies used in this study can be found in Supplementary information.

3. Results

3.1. Domain structure of IκBL for localization to nuclear speckles

Based on the domain structure and Ka/Ks value, IκBL was divided into four segments; N-terminal segment (N) (amino acids 1–66) containing a putative NLS, ankyrin repeat domain segment (A) (amino acids 67–137), central variable segment (Cv)

(amino acids 138–297), and C-terminal conserved segment (Cc) containing a leucine zipper motif (amino acids 298–381) (Fig. 1A and B). Cellular localization of IκBL was investigated in HeLa cells transfected with EGFP-tagged IκBL. As shown in Fig. 1C, IκBL-linked EGFP signal was co-localized with SC35, a member of SR protein family, in the nuclear speckles. On the other hand, HeLa cells expressing EGFP-IκBL-ΔN showed diffuse cytoplasmic EGFP signals, demonstrating that the segment N was essential for the nuclear localization. Segments A and Cv were indispensable for the nuclear localization of IκBL, because their deletions impaired the localization to the nuclear speckles. In contrast, deletion of the segment Cc had no effect on the subnuclear localization of IκBL.

3.2. *IκBL inhibits exon exclusion in alternative splicing of immune-related genes*

Localization of IκBL in the nuclear speckles, along with the evidence that genetic variations of IκBL were associated with the susceptibility to inflammatory and/or autoimmune diseases, leads to a hypothesis that IκBL might play a pivotal role in the alternative splicing of immune-related genes. Because human *CD45* gene is known to undergo alternative splicing of exons from 3 to 7, we generated a mini-gene construct for human *CD45* covering exons 3–7. The mini-gene construct was transfected into a monkey cell line COS7 with inducers of alternative splicing, hnRNPLL or hnRNPL [18–21]. In the hnRNPLL-induced *CD45* alternative splicing, IκBL decreased the generation of exons 3-7 isoform and oppositely increased the exons 3-4-5-6-7 isoform (Fig. 2A). Similar effects of IκBL on the *CD45* alternative splicing were also observed in human cell lines, HeLa and HEK293T (data not shown). In addition, it was observed that IκBL also suppressed the hnRNPL-induced alternative splicing of *CD45* (Supplementary Fig. S1).

We next examined whether the silencing of endogenous *NFKBIL1* would affect the hnRNPLL-induced *CD45* alternative splicing. *CD45* mini-gene and hnRNPLL were transfected into HeLa, in which the endogenous *NFKBIL1* was interfered by human *NFKBIL1*-specific siRNA. It was found that the knock-down of *NFKBIL1* increased the exons 3-7 isoform and concomitantly decreased the exons 3-5-7 isoform (Fig. 2B), indicating that IκBL facilitated the exon inclusion in alternative splicing of *CD45*.

To examine the effect of IκBL on other human immune-related genes, we created mini-genes of *CD72* and *CTLA4*. A *CD72* mini-gene covered exons 7 and 8, whereas a *CTLA4* mini-gene encompassed exons 2–4. The hnRNPLL-induced *CD72* alternative splicing was counteracted by the expression of IκBL (Supplementary Fig. S2A). On the other hand, hnRNPLL-induced *CD72* alternative splicing was accelerated in cells where the endogenous *NFKBIL1* was silenced (Supplementary Fig. S2B). In addition, we found a suppression of FOX1-induced *CTLA4* alternative splicing by IκBL (Supplementary Fig. S3). Furthermore, we studied which domain of IκBL was involved in the regulation of alternative splicing. It was revealed that IκBL-ΔN, -ΔA and -ΔCv failed to suppress the hnRNPLL-induced *CD45* alternative splicing, whereas -ΔCc could suppress it similar to the intact (-FL) IκBL (Fig. 2C).

3.3. *Identification of molecules interacting with IκBL by Y2H screening*

Expression of *NFKBIL1* in human tissues was examined by real-time RT-PCR. It was found that *NFKBIL1* was ubiquitously expressed with the prominent expression in spleen (Supplementary Fig. S4A). Next, a Y2H screening of human spleen cDNA library was performed to identify interacting molecules

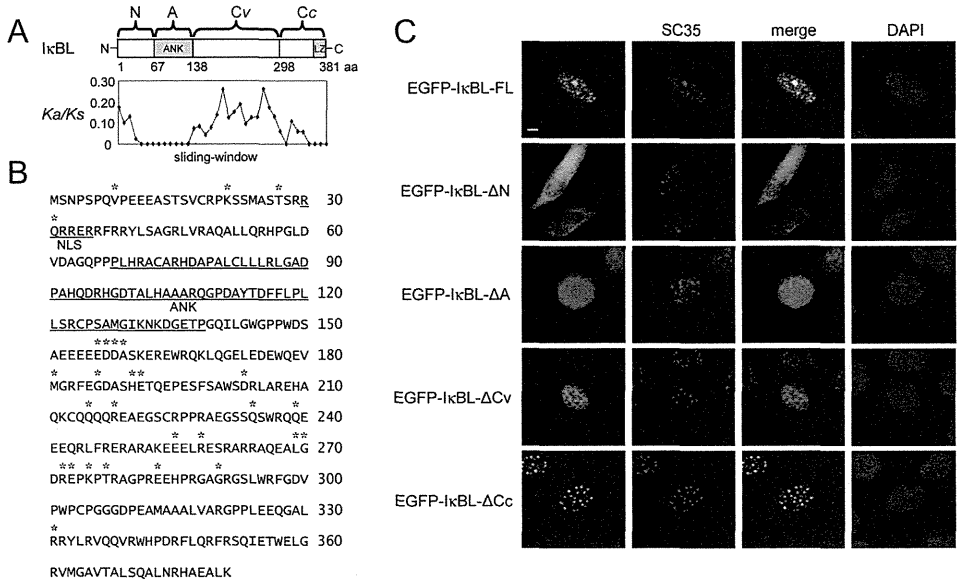

Fig. 1. Structure and cellular localization of IκBL. (A) Ka/Ks value based on the sliding window plot analysis for the *NFKBIL1* gene. Ks is the number of synonymous substitutions per synonymous site, whereas Ka is the number of nonsynonymous substitutions per nonsynonymous site, by comparing the human and murine *NFKBIL1* sequences. The Ka and the Ks values are calculated by DnaSP (v3.0). According to Ka/Ks value, IκBL was divided into four segments; N-terminal segment (N) (amino acids 1–66) containing a putative NLS, ankyrin repeats domain segment (A) (amino acids 67–137), central variable segment (Cv) (amino acids 138–297) and C-terminal conserved segment (Cc) with leucine zipper motif (amino acids 298–381). Amino acids are numbered starting from the first in-frame methionine codon. (B) Amino acid sequences of human IκBL. NLS and ankyrin repeats domain (ANK) are underlined. Asterisks indicate the positions of amino acids that are different from the amino acid sequences of murine IκBL. (C) HeLa cells were transfected with EGFP-IκBL-FL, -ΔN, -ΔA, -ΔCv or -ΔCc (EGFP signal, green) and immunofluorescence staining was performed by using anti-SC35 antibody (Alexa Fluor 568-labeled, red). IκBL-FL co-localized with SC35 in nuclear speckles. IκBL-ΔN localized in the cytosol. Both IκBL-ΔA and -ΔCv were found in the nuclei, but the localization to nuclear speckles was impaired. IκBL-ΔCc could localize to nuclear speckles, similar as IκBL-FL. A bar represents 5 μm. (For interpretation of the references to color in this figure legend, the reader is referred to the web version of this article.)

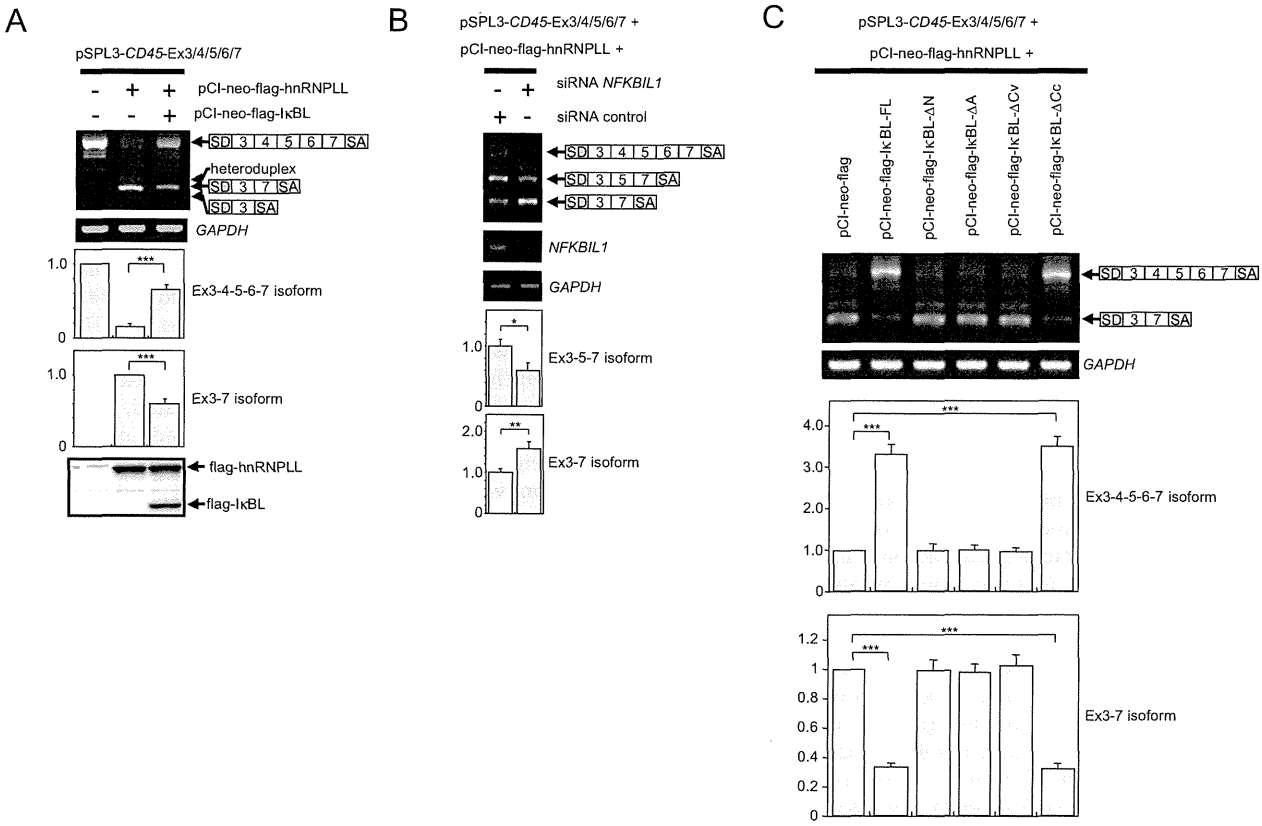

Fig. 2. Suppression of exon exclusion in the alternative splicing of *CD45* mini-gene by IκBL. (A) COS7 cells were transfected with *CD45* mini-gene and flag-hnRNPLL. RT-PCR analysis showed the effect of hnRNPLL on the alternative splicing of *CD45* transcripts derived from the mini-gene. COS7 cells were additionally transfected with flag-IκBL. The suppressive effect of IκBL on the hnRNPLL-induced alternative splicing of *CD45* is shown. Relative amounts of exons 3-4-5-6-7 isoform and exons 3-7 isoform were quantified and normalized to *GAPDH* transcripts. (B) HeLa cells were treated with siRNA specific to *NFKBIL1*, and then subjected to transfection with *CD45* mini-gene and flag-hnRNPLL. The hnRNPLL-induced alternative splicing of *CD45* was shown. Relative amounts of exons 3-5-7 isoform and exons 3-7 isoform were quantified and normalized to *GAPDH* transcripts. (C) COS7 cells were transfected with *CD45* mini-gene, flag-hnRNPLL plus one of flag-IκBL-FL, -ΔN, -ΔA, -ΔCv or -ΔCc constructs. RT-PCR analysis showed the effects of IκBL-FL, -ΔN, -ΔA, -ΔCv and -ΔCc on the hnRNPLL-induced alternative splicing of *CD45*. Relative amounts of exons 3-4-5-6-7 isoform and exons 3-7 isoform were quantified and normalized to *GAPDH* transcripts. Bar graphs in (A)–(C) represent the quantification of indicated transcripts. Data are shown as means ± SD of three replicates. $^{*}p < 0.05$; $^{**}p < 0.01$; $^{***}p < 0.005$.

with IκBL, which would provide us with useful information for the molecular mechanism of IκBL-dependent splicing regulation. A total of 11 different interacting proteins, including CLK1, were picked-up in the Y2H screening (Supplementary Fig. S4B). Interestingly, it was found that IκBL bound itself, suggesting that IκBL could form a multimer.

3.4. IκBL interacts with CLK1

The interaction of IκBL with CLK1 was further investigated, because CLK1 was known to play an important role in the alternative splicing [14–16] and the endogenous CLK1 localized in nuclear speckles (Fig. 3A). To confirm the interaction between IκBL and CLK1, COS7 were transfected with a flag-IκBL construct, followed by immunoprecipitation (IP) with an anti-CLK1 antibody and subsequent immunoblotting of IκBL using an anti-flag antibody. As shown in Fig. 3B, IκBL was found in the IP products of endogenous CLK1 and treatment with RNase A had little effect on the interaction. In addition, deletion mutants of IκBL, IκBL-ΔN, -ΔA and -ΔCv, failed to associate with CLK1 (Fig. 3C). To examine the role of CLK1 in the alternative splicing, HEK293T cells were pre-treated with siRNA to knockdown the endogenous expression level of *CLK1* (Fig. 4D). Knockdown of *CLK1* impeded hnRNPLL-induced alternative splicing of both *CD45* and *CD72*, as similar to the inhibition by IκBL (Fig. 4D and Supplementary Fig. S2C, respectively).

3.5. Regulation of alternative splicing by IκBL was independent from kinase activity of CLK1

We next asked how IκBL suppressed the exon skipping in alternative splicing. Given that IκBL interacted with CLK1, and knockdown of *CLK1* impeded alternative splicing, IκBL might inhibit the function of CLK1. CLK1 is composed of N-terminal regulatory domain and C-terminal kinase domain (Supplementary Fig. S5A) and is known to phosphorylate SR proteins, which are involved in the splicing. COS7 were transfected with a myc-tagged construct for an SR protein, ASF/SF2, with or without CLK1 full-length (CLK1-FL) or kinase domain deleted (CLK1-Δkinase) constructs. It was confirmed that the kinase domain was indispensable for CLK1 to phosphorylate ASF/SF2, whereas IκBL failed to affect the CLK1-induced phosphorylation of ASF/SF2 (Fig. 4A). On the other hand, the functional domain of CLK1 indispensable for the regulation of alternative splicing in *CD45* was, to our surprise, the N-terminal regulatory domain, but not the kinase domain (Supplementary Fig. S5B). These data indicated that both IκBL and CLK1 regulated the alternative splicing of *CD45*, in which the kinase activity of CLK1 was not involved.

N-terminal regulatory domain of CLK1 was reported to interact with ASF/SF2 [14], and we confirmed that N-terminal domain of CLK1 bound ASF/SF2 (Supplementary Fig. S6A). On the other hand, when we transfected COS7 with constructs of flag-ASF/SF2-FL, -ΔRRM1β1, -ΔRRM2β1, -ΔRRM1&2β1 or -ΔRS, followed by